OFFICE OF NAVAL RESEARCH

Contract N00014-86-K-0639

R&T Code 4133013...2

Technical Report No. 9

Nanosecond Molecular Dynamics and Vibrational Spectra of Li^+-Chain-Polyethers in Acetonitrile

by

J. Eschmann, J. Strasser, M. Xu, Y. Okamoto,
Edward M. Eyring and Sergio Petrucci

Prepared for Publication

in

Journal of Physical Chemistry

University of Utah
Department of Chemistry
Salt Lake City, UT 84112

June 27, 1989

Unclassified
SECURITY CLASSIFICATION OF THIS PAGE

REPORT DOCUMENTATION PAGE

1a. REPORT SECURITY CLASSIFICATION Unclassified	1b. RESTRICTIVE MARKINGS
2a. SECURITY CLASSIFICATION AUTHORITY	3. DISTRIBUTION / AVAILABILITY OF REPORT Approved for public release and sale. Distribution unlimited.
2b. DECLASSIFICATION / DOWNGRADING SCHEDULE	
4. PERFORMING ORGANIZATION REPORT NUMBER(S) ONR Technical Report No. 9	5. MONITORING ORGANIZATION REPORT NUMBER(S)
6a. NAME OF PERFORMING ORGANIZATION University of Utah 6b. OFFICE SYMBOL (If applicable)	7a. NAME OF MONITORING ORGANIZATION
6c. ADDRESS (City, State, and ZIP Code) Department of Chemistry University of Utah Salt Lake City, UT 84112	7b. ADDRESS (City, State, and ZIP Code)
8a. NAME OF FUNDING / SPONSORING ORGANIZATION Office of Naval Research 8b. OFFICE SYMBOL (If applicable) ONR	9. PROCUREMENT INSTRUMENT IDENTIFICATION NUMBER N00014-86-K-0639
8c. ADDRESS (City, State, and ZIP Code) 800 N. Quincy St. Arlington, VA 22217	10. SOURCE OF FUNDING NUMBERS PROGRAM ELEMENT NO. / PROJECT NO. / TASK NO. / WORK UNIT ACCESSION NO

11. TITLE (Include Security Classification)
Nanosecond Molecular Dynamics and Vibrational Spectra of Li^+-Chain-Polyethers in Acetonitrile

12. PERSONAL AUTHOR(S)
J. Eschmann, J. Strasser, M. Xu, Y. Okamoto, E. M. Eyring and S. Petrucci

13a. TYPE OF REPORT	13b. TIME COVERED	14. DATE OF REPORT (Year, Month, Day)	15. PAGE COUNT
Technical	FROM 9/87 TO 6/89	1989, June 27	53

16. SUPPLEMENTARY NOTATION
Prepared for publication in the Journal of Physical Chemistry

17 COSATI CODES			18 SUBJECT TERMS (Continue on reverse if necessary and identify by block number)
FIELD	GROUP	SUB-GROUP	Lithium Arsenic Hexafluoride
	approx.		

19 ABSTRACT (Continue on reverse if necessary and identify by block number) Lithium Perchlorate

Ultrasonic relaxation spectra in the 1-500 MHz frequency range for $LiClO_4$ or $LiAsF_6$ (0.03 to 1 M) added to open chain polyethers (triglyme) in molar ratio R=1, or added to poly-(ethylene oxide) in molar ratio $R_{(PEO)}$ = [(-CH_2-CH_2-O-)]/[Li^+] = 4, in the solvent acetonitrile at 25°C are reported. The spectra were interpreted by the sum of two Debye relaxation processes. The remarkable finding is that the relaxation times are independent of the chain length in going from triglyme at R=1 to a poly(ethylene oxide) of 15,000 average molar weight at $R_{(PEO)}$ = 4. The observed processes appear to reflect a localized cation-polyether interaction (here dubbed the "ether moiety effect"). The relaxations are interpreted by an Eigen-Winkler mechanism in which a cation-ether contact is followed by the polyether chain wrapping around the Li^+ ion. Specific effects in the ultrasonic absorption amplitudes differentiating the spectra of triglyme from the polyether spectra are reported.

(over)

20. DISTRIBUTION / AVAILABILITY OF ABSTRACT	21. ABSTRACT SECURITY CLASSIFICATION
☐ UNCLASSIFIED/UNLIMITED ☐ SAME AS RPT ☐ DTIC USERS	Unclassified
22a NAME OF RESPONSIBLE INDIVIDUAL Edward M. Eyring	22b. TELEPHONE (Include Area Code) (801) 581-8658 / 22c. OFFICE SYMBOL

19. Abstract (continued):

Infrared spectra between 800 and 900 cm^{-1} of the same systems show cation-ether vibrations due to cage effects. The infrared spectral envelopes of both the polyethers alone and the polyether added to Li^+ are deconvoluted by three Gaussian-Lorentzian bands. For triglyme a weak band at 879 cm^{-1} is strongly enhanced in absorbance and shifted to 870 cm^{-1} when Li^+ is present. This band is attributed to wrapping of the polyether glyme around the cation. Since no significant infrared band enhancement is observed for poly(ethylene oxide) in acetonitrile, it is possible that the same configuration is hindered for long polyether chains.

Ultrasonic and infrared spectra for the cyclic polyether 12-crown-4 in the presence of Li^+ in acetonitrile are reported for comparison. For 12C4 + Li^+, the ultrasonic spectrum can be interpreted by the sum of two Debye relaxation processes. The first at lower frequencies has a lower relaxation frequency (by a factor of ~5) than the one present in triglyme. This may reflect the more rigid ring structure of 12C4 opposing the entrance of the cation and thus altering (enthalpically or entropically) the activation free energy of the complexation process. The infrared spectrum of 12C4 in the 800-900 cm^{-1} region can be deconvoluted by four Gaussian-Lorentzian bands, two of which dominate the absorbance. Addition of Li^+ in molar ratio R = [macrocycle]/[Li^+] = 0.5 shifts dramatically both the position and relative intensity of the infrared bands of the crown-ether.

Nanosecond molecular dynamics and vibrational spectra of Li^+-chain-polyethers in acetonitrile

by

J. Eschmann, J. Strasser, M. Xu, Y. Okamoto, Edward M. Eyring and S. Petrucci*

Weber Research Institute, Polytechnic University, Long Island Center, Route 110, Farmingdale, NY 11735, and Department of Chemistry, University of Utah, Salt Lake City, UT 84112

Abstract

Ultrasonic relaxation spectra in the 1-500 MHz frequency range for $LiCl O_4$ or $LiAsF_6$ (0.03 to ~1 M) added to open chain polyethers (triglyme) in molar ratio R=1, or added to poly(ethylene oxide) in molar ratio R_{PEO} = [(-CH_2-CH_2-O-)]/[Li^+] = 4, in the solvent acetonitrile at 25°C are reported. The spectra were interpreted by the sum of two Debye relaxation processes. The remarkable finding is that the relaxation times are independent of the chain length in going from triglyme at R=1 to a poly(ethylene oxide) of 15,000 average molar weight at R_{PEO} = 4. The observed processes appear to reflect a localized cation-polyether interaction (here dubbed the "ether moiety effect"). The relaxations are interpreted by an Eigen-Winkler mechanism in which a cation-ether contact is followed by the polyether chain wrapping around the Li^+ ion. Specific effects in the ultrasonic absorption amplitudes differentiating the spectra of triglyme from the polyether spectra are reported.

Infrared spectra between 800 and 900 cm^{-1} of the same systems show cation-ether vibrations due to cage effects. The infrared spectral envelopes of both the polyethers alone and the polyether added to Li^+ are deconvoluted by three Gaussian-Lorentzian bands. For triglyme a weak band at 879 cm^{-1} is strongly enhanced in absorbance and shifted to 870 cm^{-1} when Li^+ is present. This band is attributed to wrapping of the polyether glyme around the cation. Since no significant infrared band enhancement is observed for poly(ethylene oxide) in acetonitrile, it is possible that the same configuration is hindered for long polyether chains.

Ultrasonic and infrared spectra for the cyclic polyether 12-crown-4 in the presence of Li^+ in acetonitrile are reported for comparison. For 12C4 + Li^+, the ultrasonic spectrum can be interpreted by the sum of two Debye relaxation processes. The first at lower frequencies has a lower relaxation frequency (by a factor of ~5) than the one present in triglyme. This may reflect the more rigid ring structure of 12C4 opposing the entrance of the cation and thus altering (enthalpically or entropically) the activation free energy of the complexation process. The infrared spectrum of 12C4 in the 800-900 cm^{-1} region can be deconvoluted by four Gaussian-Lorentzian bands, two of which dominate the absorbance. Addition of Li^+ in molar ratio R = [macrocycle]/[Li^+] = 0.5 shifts dramatically both the position and relative intensity of the infrared bands of the crown-ether.

Introduction

The mechanism of complexation of cyclic polyethers with alkali ions in aqueous and nonaqueous solutions has been studied extensively by ultrasonic, NMR and stopped flow techniques.[1] In media of relatively high permittivity (where anion competition for the first coordination shell of the cation is negligible) the Eigen-Winkler mechanism:[2]

$$M + C \underset{k_{-o}}{\overset{k_o}{\rightleftharpoons}} M...C \underset{k_{-1}}{\overset{k_1}{\rightleftharpoons}} MC \underset{k_{-2}}{\overset{k_2}{\rightleftharpoons}} (MC)$$

appears to rationalize successfully most of the kinetic data. The present paper extends this kinetic research to open chain polyethers and to polymers. Justifications for such a study include the wish to understand the "macrocyclic effect"[3] (namely the ring effect, whether enthalpic or entropic) on the rate of ion complexation. Elongating the open polyether chain yields data relevant both to biological systems and to new, thin film, polymeric battery electrolytes.

Ultrasonic relaxation techniques,[4] covering the 1-500 MHz frequency range (0.3 ns to 160 ns), have proven to be particularly suitable tools for this kinetic investigation.

Infrared (IR) spectra have been obtained in the 800 to 900 cm^{-1} region because polyethers in the presence of cations have shown Raman absorption bands which were ascribed[5] to the cation vibrating in an ethereal solvation-cage. Since Li^+ vibrates against a solvent cage at ~ 400 cm^{-1},[6] the bands at 800-900 cm^{-1} are similar in nature to the far-IR bands now appearing in the IR spectrum for polyether-ligands.

Experimental

The equipment and procedures for the ultrasonic and IR work have been described elsewhere.[1,7] $LiCl O_4$ (Aldrich) and $LiAsF_6$ (Agri. Chem. Co.) were dried at 70°C *in vacuo* for several hours to constant weight. Acetonitrile (Aldrich, gold label) was distilled over P_2O_5 after refluxing the liquid for a few hours. Triglyme (Aldrich) was distilled *in vacuo* in an all Pyrex column without grease on the joints. Poly(ethylene oxide) (MW $\sim$ 15,000) was prepared in Dr. Okamoto's laboratory. It was dried *in vacuo* to constant weight at room temperature before use. Solutions of electrolytes and polyethers were prepared by weight, bringing the solution to volume in volumetric flasks with distilled acetonitrile, after dissolving the solute in the same solvent. Contact with the atmosphere during preparation of the solutions and filling of the cells was kept to a minimum ($\sim$ 30 seconds overall).

For polymeric solutions the $(-CH_2-CH_2-O-)$ moiety was the "molar mass unit." Hence solutions reported as $R_{PEO} = 4$ have a composition $[(-CH_2-CH_2-O-)]/[LiX] = 4$ where X denotes the anion. A solution of triglyme $[CH_3(-O-CH_2-CH_2)_3-OCH_3]/[LiX] = 1$ is equivalent to a polymer solution at $R_{PEO} = 4$ that can be depicted as $(-CH_2-CH_2-O-)_4/LiX$ with the same oxygen atom to Li^+ ratio.

Results and Calculations

a) Ultrasonic Relaxation Kinetics

Figures 1A and 1B are representative ultrasonic absorption spectra of $LiClO_4$ + Triglyme and $LiClO_4$ + PEO, respectively, in acetonitrile at 25°C. The ultrasonic spectra are expressed in terms of the function μ, the excess sound absorption per wavelength,[4]

$$\mu = \alpha_{exc} \lambda = (\alpha - Bf^2) \frac{u}{f} \qquad (1)$$

where the wavelength $\lambda = \frac{u}{f}$ with u denoting the sound velocity and f the frequency. Here α is the sound attenuation coefficient at the frequency f. B is the value of $\frac{\alpha}{f^2}$ at frequencies much higher than the relaxation frequency(ies) of the process(es) under study.

The solid line in these ultrasonic absorption spectra is μ evaluated as the sum of two Debye relaxation processes[3]

$$\mu = 2\mu_I \frac{f/f_I}{1+(f/f_I)^2} + 2\mu_{II} \frac{f/f_{II}}{1+(f/f_{II})^2} \qquad (2)$$

with μ_I and μ_{II} the maximum excess sound absorptions per wavelength at the respective relaxation frequencies f_I and f_{II}. The insets of Figs. 1A and 1B report the tail of the relaxation processes expressed by α/f^2 vs f where the solid line is eq. 2 rearranged[3] to read

$$\frac{\alpha}{f^2} = \frac{A_I}{1+(f/f_I)^2} + \frac{A_{II}}{1+(f/f_{II})^2} + B \qquad (3)$$

with $A_I = 2\mu_I/f_I u$ and $A_{II} = 2\mu_{II}/f_{II} u$. Table I (microfilm edition) reports the parameters μ_I, f_I, μ_{II}, f_{II}, B and the sound velocity u. These five parameters were calculated by a computer-graphic fit of eqs. 2 and 3 to the experimental values α/f^2 and μ vs. f data. Estimated average errors are $\pm$ 5% for the μ values, $\pm$ 2 MHz for the $f_{I,II}$ values, and $\pm$ 1 x 10^{-17} cm^{-1} s^2 for B while the sound velocities are affected by an experimental average error of $\pm$ 1%.

Figures 2A and 2B report the values of u and of B vs concentration for the various systems investigated. Specific effects appear for u depending on the electrolyte and independent of the polyethers. On the other hand, B values seem to show specificity for both anion and polyether with increasing concentration. Apparently, the electrolyte influences the adiabatic compressibility $\beta_s = \frac{1}{\rho u^2}$ through the sound velocity u where $\rho \equiv$ density.

Both the shear viscosity η_s and the bulk compressional viscosity η_v of the liquids are affected by the polyethers and the anions

$$\frac{\alpha}{f^2} = \frac{2\pi^2}{\rho u^3}\left(\frac{4}{3}\eta_s + \eta_v\right) \qquad (4)$$

since the value of $\left(\frac{\alpha}{f^2}\right)_{f>>f_I,f_{II}} = B$ is displaced by changes in polyether and anion concentrations.

Figure 3A reports the inverse of the relaxation times for the "fast" process, $\tau_I^{-1} = 2\pi f_I$, plotted vs. the concentration of the electrolyte. The significant features of this plot are a leveling to a plateau of the τ_I^{-1} values with increasing concentration and the independence of the results of the nature of the ligand (triglyme or POE) as well as of the type of anion present ($C\ell O_4^-$ or AsF_6^-). A solution containing either of the electrolytes alone or either of the polyethers alone does not show any ultrasonic relaxation. Thus the observed effect is due to the interaction of Li^+ with the polyethers. This interaction is local in the sense that each Li^+ interacts with a local section of the PEO (one or more oxygens of the four available per Li^+ atom) and ignores the next segment + Li^+ interaction. We have chosen to call this the "ether moiety effect". This would explain the equality of the ultrasonic results for Li^+ + PEO with those for Li^+ + TG (TG ≡ triglyme) in the solvent acetonitrile.

Figure 3B is a plot of $\tau_{II}^{-1} = 2\pi f_{II}$ for the "slow" process vs. the concentration of the electrolyte. The same qualitative behavior as for τ_I^{-1} vs. concentration is observed with the data tending asymptotically toward a constant value at high concentration and showing independence of

the nature of either the polyether or anion within experimental error (except for two points at 0.1 and 0.5 M). Hence the same general conclusions reached for the "fast" process also apply here.

On the basis of the above observations, we propose a mechanism of the Eigen-Winkler type[2] wherein Li^+ and the polyether (or a segment of it in the case of PEO) approach each other, presumably by a diffusion controlled process, followed by a first encounter involving partial desolvation of Li^+ ion and contact with one oxygen atom of the polyether. This process is then followed by the polyether wrapping around the completely desolvated Li^+ ion. This sequence of events can be represented by the scheme:

$$Li^+ + TG \underset{\hat{k}_{-o}}{\overset{k_o}{\rightleftarrows}} Li^+ \ldots TG \underset{\hat{k}_{-1}}{\overset{k_1}{\rightleftarrows}} LiTG^+ \underset{\hat{k}_{-2}}{\overset{k_2}{\rightleftarrows}} (LiTG)^+ \qquad (5)$$

which at high concentrations, when $[Li^+]$ and [TG] become relatively very small, is reduced to a pseudo first-order scheme

$$Li^+ \ldots TG \underset{\hat{k}_{-1}}{\overset{k_1}{\rightleftarrows}} LiTG^+ \underset{\hat{k}_{-2}}{\overset{k_2}{\rightleftarrows}} (LiTG)^+ \qquad (6)$$

that is observed experimentally.

In the above mechanisms, TG can be replaced by a segment of PEO. Also, $Li^+ \ldots TG$ represents a solvent separated species, whereas $LiTG^+$ and $(LiTG)^+$ symbolize the contact and the "wrapped" complex respectively. From scheme (5), following Eigen and Tamm,[8] it follows that for the "fast" process:

$$\tau^{-1}_{I} = k_1 \frac{\theta}{\theta + K_{-o}} + k_{-1} = k_1 \phi + k_{-1} \qquad (7)$$

with $\theta \simeq 2\sigma C$ where σ is the degree of dissociation of the complex $(LiTG)^+$. Thus the observed "fast" relaxation corresponds to the second step of scheme (5) coupled to the one with $K_{-o} = \frac{k_{-o}}{k_o}$, the inverse of the equilibrium constant of the first step. At high enough concentration, one can predict that $\theta >> K_{-o}$ and $\phi \to 1$ giving

$$\tau^{-1} = k_1 + k_{-1} \qquad (8)$$

whereas as $C \to 0$ $\qquad \tau_I^{-1} = k_{-1} \qquad (9)$

Condition (8) is achieved experimentally, as shown in Fig. 3A, giving $\tau_I^{-1} = k_1 + k_{-1} = 6._3 \times 10^8\ s^{-1}$. Taking the data at $C < 0.15$ M for Li^+ + PEO, namely $\tau^{-1} \times 10^{-8}\ (s^{-1}) = 2.83$, 3.46, 4.40 and 5.66 for $C = 0.05$, 0.076, 0.10 and 0.15 M respectively, by linear regression one obtains the determination coefficient $r^2 = 0.99_3$, intercept $I = 1._4 \times 10^8$, and slope $S = 2.8_8 \times 10^9$. Thus for the first step of scheme (6): $k_{-1} = 1._4 \times 10^8\ s^{-1}$, $k_1 = 4._9 \times 10^8\ s^{-1}$ and $K_1 = (k_1/k_{-1}) = 3._5$ From scheme (5), following Eigen and Tamm,[8] one can write for the "slow" process:

$$\tau_{II}^{-1} = k_2 \frac{\phi}{\phi + K_{-1}} + k_{-2} \qquad (10)$$

where $K_{-1} = (3.5)^{-1} = 0.29$.

At high enough concentrations, one can have the condition $\phi = 1$, and:

$$\frac{\phi}{\phi+K_{-1}} = \frac{1}{1.3} = 0.7_7.$$

Therefore $\tau_{II}^{-1} = 0.7_7\, k_2 + k_{-2} \simeq 10._4 \times 10^7\ s^{-1}$ as taken from the asymptotic value of τ_{II}^{-1} (Fig. 3B). Also, from the data for Li^+ + PEO at $C \leq 0.20$, namely $\tau_{II}^{-1} \times 10^7(s^{-1}) = 1.7_6, 2.5_1, 4.4_0, 4.7_1, 5.6_5$ at the concentrations $C = 0.05, 0.07_6, 0.1_0, 0.1_5, 0.20$ (mol/dm^3) respectively, by linear regressions, one obtains $r^2 = 0.88$, intercept $I = 9._1 \times 10^6$, and slope $S = 2.5 \times 10^8$.

Thus for the slow step of scheme (6): $k_{-2} = 9 \times 10^6\ s^{-1}$, $k_2 = (10._4 - 0.9)10^7/0.77 = 1._2 \times 10^7\ s^{-1}$ and $K_2 = (k_2/k_{-2}) = 13$.

The overall formation constant K_Σ is related to the formation constants of the various steps by:

$$K_\Sigma = K_o(1+K_1+K_1K_2), \qquad (11)$$

leading in this case to the numerical result: $(K_\Sigma/K_o) = 1 + K_1 + K_1K_2 = 50$.

From these calculations it follows that forward and reverse rate constants and equilibrium constants of scheme (6) are independent of the length of the

poly(ethylene oxide) chains at an oxygen to Li^+ ratio = 4 in the solvent CH_3CN.

Examination of the values of μ_I and μ_{II} reported in Table I further illuminates the situation. Figure 4A is a plot of μ_I, the excess sound absorption coefficient per wavelength, for the "fast" process plotted vs. the concentration of electrolyte. The data show a strong dependence on the nature of the polyether ligand.

Following Eigen and Tamm,[8] scheme (5) can be rewritten as

$$\underset{C_0}{Li^+} + \underset{C_0}{PEO} \overset{K_0}{\underset{}{\rightleftharpoons}} \underset{C_1}{Li^+...PEO} \overset{K_1}{\rightleftharpoons} \underset{C_2}{LiPEO^+} \overset{K_2}{\rightleftharpoons} \underset{C_3}{(LiPEO)^+} \qquad (12)$$

where PEO denotes here the segment of the polymer reacting with a particular Li^+ ion.

From the above, $C = C_0 + C_1 + C_2 + C_3 \simeq C_1 + C_2 + C_3$, neglecting C_0 ($C_0 \ll C_1, C_2, C_3$). Then:

$$\mu_I = \frac{\pi}{2\beta_s} \frac{\Delta V_I^2}{RT} \left[\frac{1}{C_1} + \frac{1}{C_2}\right]^{-1} = \frac{\pi}{2\beta_s} \frac{\Delta V_I^2}{RT} \Gamma_I^{-1}. \qquad (13)$$

The calculation of C_1, C_2, C_3, and hence of Γ_I^{-1} has been done by using the relations: $C \simeq C_1 + C_2 + C_3$, $K_1 = (C_2/C_1) = 3.5$ and $K_2 = (C_3/C_2) = 13.5$. Figure 5A is a plot of μ_I vs. Γ_I^{-1} data for $LiClO_4$ + PEO and $LiAsF_6$ + PEO for $C \leq 0.5$ M. Linear regression, giving 50% statistical weight to the

origin, gives $r^2 = 0.994$, an intercept $I_I = 6._9 \times 10^{-5}$, and a slope $S_I = 942.2$ from which, given $\beta_s = (\rho \bar{u}^2)^{-1} = [0.777 \times (1.27_9 \times 10^5)^2]^{-1} = 78._6 \times 10^{-12}$, it follows that

$$\Delta V_I = [\frac{2\beta_s RT}{\pi} S_1]^{1/2} = 34._2 \text{ cm}^3/\text{mole}.$$

The μ_I data in the plot of μ_I vs. C for Li^+ + TG appear to be too small in value to attempt a correlation with Γ_I^{-1}, requiring a slope to evaluate ΔV_I.

Figure 4B is a plot of μ_{II} vs. C, (the excess sound absorption per wavelength for the "slow" process vs. concentration) for all the systems investigated. One notices (as for the corresponding plot of μ_I vs C) a saturation or tendency to saturation of μ_{II} with C, thereafter μ_{II} becoming independent of C. In addition, whereas all the data of $LiCl\ell O_4$ + TG, $LiCl\ell O_4$ + PEO and $LiAsF_6$ + TG seem to fall on a common line, the data for $LiAsF_6$ + PEO diverge, and they follow their own saturation trend. This anion specificity, for longer chain polyethers, will be investigated later.

For the moment we will focus on the data for Li^+ + PEO ($LiCl\ell O_4$ + PEO] at $C \leq 0.32$ M. Following Eigen and Tamm,[8] for process (6):

$$\mu_{II} = \frac{\pi}{2\beta_s} \frac{\Delta V_{II}^2}{RT} [\frac{1}{C_1+C_2} + \frac{1}{C_3}]^{-1} = \frac{\pi}{2\beta_s} \frac{\Delta V_{II}^2}{RT} \Gamma_{II}^{-1} \qquad (14)$$

Figure 5B reports the data for μ_{II} plotted vs. the calculated Γ_{II}^{-1}. Linear regression applied to the linear portion of the plot of the $LiClO_4$ + PEO data for $C \leq 0.32$ M, assigning 50% statistical weight to the origin, gives $r^2 = 0.98$, an intercept $I_{II} = 6._1 \times 10^{-5}$, and a slope $S_{II} = 144$, from which it follows that

$$\Delta V_{II} = \left[\frac{2\beta_s RT}{\pi} S_{II}\right]^{1/2} = 13.4 \text{ cm}^3/\text{mole}.$$

b) Infrared Spectra

Figure 6A is the infrared spectrum in the 800-900 cm^{-1} region of triglyme 0.6 M in acetonitrile. The spectral envelope can be deconvoluted by three Gaussian-Lorentzian semiempirical product functions[9] (dashed lines):

$$A_j = A_j^o \left[\exp\left(-\frac{(\bar{\nu}-\bar{\nu}_j^o)^2}{2\sigma^2}\right)\right]\left[1 + \frac{(\bar{\nu}-\bar{\nu}_j^o)^2}{\sigma_j^2}\right]^{-1} \qquad (15)$$

where A_j^o is the absorbance at the peak of the band centered at the wavenumber $\bar{\nu}_j^o$, $\bar{\nu}$ is the wavenumber (cm^{-1}) and σ_j^2 is the variance, with the standard error $\sigma_j = \frac{(\Delta\bar{\nu}_{1/2})_j}{1.46}$. $(\Delta\bar{\nu}_{1/2})_j$ is the width of the function at $A^o_j/2$.

Addition of either 0.6 M $LiClO_4$ or 0.6 M $LiAsF_6$ (Figs. 6B and 6C) in molar ratio R=1 causes a shift of the spectrum to lower wavenumbers and strong enhancement of the higher frequency band, which now appears at 870 cm^{-1}.

Previous workers[5] noted a similar appearance of bands at 800-900 cm^{-1} upon addition of alkali ions to polyethers including macrocycles. These bands were attributed[5] to vibration of the ion inside an ethereal wrap-around cage similar to the far infrared spectra of alkali vibrating against a solvent cage[6] (~400 cm^{-1} for Li^+).

A similar interpretation is given here to the band at 870 cm^{-1} for Li^+ + triglyme. The normalized absorbances at unit cell length A^o_j/ℓ for triglyme and Li^+ + triglyme are reported in Figs. 7A and 7B. The band at 870 cm^{-1} (with an amplitude independent of the nature of the anion) is shown in Fig. 7B to be very much enhanced with respect to the one at 874 cm^{-1} for pure triglyme in CH_3CN. Thus for Li^+ + triglyme there is structural evidence that correlates nicely with the dynamic spectra produced by ultrasonic relaxation techniques.

The situation is not so straightforward when the infrared spectra of PEO and of Li^+ + PEO are considered. Figures 8A, 8B and 8C report the infrared spectral profiles of the digitized spectra for PEO, $LiClO_4$ + PEO

and $LiAsF_6$ + PEO, respectively, in the 800-900 cm^{-1} region. Again, three Gaussian-Lorentzian functions (dashed lines) can describe the spectra (solid lines in Figs. 8A, 8B, and 8C). However, in the present case, no strong enhancement of bands occurs with the exception of a modest increase of the band at 811-813 cm^{-1} which appears also to be anion dependent.

Figures 9A, 9B, and 9C compare the normalized absorbances A^o_j/ℓ per unit length of cell for the three bands for PEO alone and for the two electrolyte solutions. Consistent with the above observations, the electrolyte does seem to depress the value of A_j^o/ℓ for the two upper bands at ~ 864 and 845 cm^{-1}. Evidently, for long chain polyethers, the structural configuration that causes the appearance of a new or enhanced band when Li^+ is present does not form. Thus, in this respect there is no correspondence between the information deduced from ultrasonic absorption spectra (very similar for TG and PEO) and the information derived from the infrared spectra.

All the parameters required for the deconvolution of the spectral envelopes by eq. 15 are reported in Table II (microfilm edition).

c) <u>Comparison with macrocycle - lithium ion interactions in solutions of $LiClO_4$ + 12C4 in acetonitrile</u>.

A comparison of the above results, gathered on Li^+ interacting with triglyme, with corresponding information for Li^+ interacting with the cyclic macrocycle 12C4 could conceivably illuminate both systems. 12-crown-4 is

the macrocycle that corresponds to the acyclic triglyme since both have four oxygen atom electron donors per molecule:

Figure 10A is the ultrasonic absorption spectrum of $LiC\ell O_4$ 0.3 M + 12C4 0.3 M in acetonitrile at 25°C plotted as μ vs f. Two Debye relaxation processes adequately describe the spectrum. Whereas the upper relaxation has a frequency comparable to that reported above for $LiC\ell O_4$ + TG, the lower relaxation frequency for $LiC\ell O_4$ + 12C4 is about 5 times smaller at C = 0.3 M than the corresponding relaxation frequency for $LiC\ell O_4$ + TG in acetonitrile.

Assuming either scheme 5 or 6 also applies for the Li^+ + 12C4 system, the qualitative conclusion to be drawn is that the free energy of activation barrier $\Delta G^{\neq}_{II}$, for the "slow" process, is greater for 12C4 than that for the triglyme. It remains to be established whether this difference has an enthalpic or entropic origin, although the rigidity of the 12C4 polyether ring compared to the flexible TG, would appear to play a leading role in the relative ease of cation encapsulation. The fitted parameters μ_I, f_I, μ_{II}, f_{II}, B and the sound velocity u for $LiC\ell O_4$ 0.3 M + 12C4 0.3 M in acetonitrile at 25°C, are reported in Table I (microfilm edition).

Figure 10B is a representative infrared spectrum in the 800-900 cm^{-1} region for 12C4 in the solvent acetonitrile, expressed in absorbance A *vs.* wavenumber $\bar{\nu}(cm^{-1})$. The spectral envelope has been deconvoluted into three Guassian-Lorentzian product functions, eq. 15. From Fig. 10B it is evident that the two bands centered at $\bar{\nu}_o \simeq 851$ cm^{-1} and $\bar{\nu}_o \simeq 844$ cm^{-1} are the dominant components of the spectral envelope. A third band centered at $\bar{\nu}_o \simeq 833$ cm^{-1} is invisible at C = 0.2 M, but becomes evident at higher concentrations. A fourth satellite band appears at $\bar{\nu}_o = 815$ cm^{-1}. These results may indicate the presence of two predominant conformers in solution associated with $\bar{\nu}^o \simeq 851$ and $\bar{\nu}^o = 844$ cm^{-1}, respectively. For all the macrocyclic systems investigated, the parameters $\bar{\nu}_j{}^o$, $A^o{}_j$ $(\Delta\bar{\nu}_{1/2})_j$ and calibrated cell lengths are reported in Table II (microfilm edition). Figure 11A reports the absorbances $A_j{}^o$, normalized by the cells lengths ℓ, as functions of the total concentration of the crown ether in CH_3CN. The solid lines, in Fig. 11A, have been calculated by fitting cubic polynomials $(A_j{}^o/\ell) = \alpha + \beta C + \gamma C^2 + \delta C^3$ to the $(A_j{}^o/\ell)$ *vs.* concentration C data. The parameters α, β, γ and δ are reported in Table II (microfilm edition), together with the determination coefficients r^2.

Qualitative similarities and differences between the spectra of 12C4 and those of triglyme and of PEO in CH_3CN should be noted. The spectral

profiles of all of the three species at low concentrations are interpretable by three Gaussian-Lorentzian bands, although both the positions $\bar{\nu}_j^o$ and the spectral absorbances A^o_j are different for the three different species.

Figure 10C shows a representative digitized infrared spectrum of $LiC\ell O_4$ + 12C4 in the 800-900 cm^{-1} region in molar ratio $R = \frac{[12C4]}{[LiC\ell O_4]} = 0.50$. Below this value of the ratio the spectral profile remained constant (at the same concentration of 12C4), a sign of saturation of the crown ether by the cation Li^+.

Figure 10C shows a dramatic change in the wavenumber, number of bands, and the relative absorbance A_j^o of both of the two major bands of 12C4 in acetonitrile (Fig. 10B). The relative shift in absorbance of the bands suggests the predominance of one configuration when Li^+ is present, probably that with the Li^+ cation imbedded in the cavity of 12C4.

Table II displays the results in terms of the parameters $\bar{\nu}_j^o$, A_j^o and $(\Delta\bar{\nu}_{1/2})$, for the deconvoluted infrared spectra of $LiC\ell O_4$ + 12C4 at molar ratio R = 0.5 in acetonitrile. Figure 11B reports the normalized absorbances A_j^o/ℓ *vs.* concentration for $LiC\ell O_4$ + 12C4 at R = 0.5 in acetonitrile. As in the case of Li^+ + TG, presented above, unambiguous evidence for the interaction between Li^+ and the polyether 12C4 is seen

here, possibly of the same nature, namely Li^+ vibrating against the ethereal cage of the cyclic cavity.

d) Influence of the polymer chain length on the ultrasonic relaxation spectra and on the IR spectra.

The changes of μ_I from triglyme to PEO (15,000) as shown in Fig. 4A were of interest. Also the changes in μ_{II} shown for $LiAsF_6$ + PEO, with respect to the other systems (Fig. 4B), clearly indicate an anion effect as mentioned above. To clarify this result we have recorded ultrasonic spectra of $LiAsF_6$ 0.50 M + tetraglyme 0.50 M and of $LiAsF_6$ + PEO of average molar mass 400, 1000, 2000 in molar ratio $R = \frac{[(-CH_2-CH_2-O-)]}{[Li^+]} = 4$ in acetonitrile at 25°C.

The spectra were interpreted by the sum of two Debye relaxation processes. The parameters for the fit, namely μ_I, f_I, μ_{II}, f_{II}, B and the sound velocity u are reported in Table III (microfilm edition). The most salient effect associated with chain length is reported in Fig. 12 where μ_I and μ_{II} are replotted vs. average molar mass.

It can be seen that μ_I increases from the value in triglyme to the value for PEO (15,000), the larger initial increase occurring for $\bar{M} < 1000$. Similarly, the values of μ_{II} decrease rapidly for $\bar{M} < 1000$ and reach a plateau. Whereas the first effect for μ_I is associated with the chain

length of the polymer, the second effect for μ_{II} is also dependent on the anion, the effect of decreasing μ_{II} with increasing $\bar{M}$ not being present for $LiClO_4$. As the relaxation frequencies, the rate constants and the equilibrium constants are not affected by either chain length or anion, the above effects seem to be linked to ΔV_I and ΔV_{II}, namely to the isoentropic volume changes of reaction. The specific molecular mechanisms of this behavior are not apparent at the present time. The anion dependence of μ_{II} may reflect some steric hindrance to the complete wrapping of the polyether chain about the cation (due to the presence of the anion AsF_6^-), which increases rapidly with increasing polyether chain length. Notice, in fact, from Fig. 4B, that the effect of μ_{II} diverging from the common behavior is specific for $LiAsF_6$ in PEO; hence it is an anion effect associated with the length of the polyether chain.

An effect also dependent on the chain length is detectable from the IR spectra of the same systems in the 910-780 cm^{-1} region. Table IV (microfilm edition) reports the infrared parameters for the systems tetraglyme 0.5 M + $LiAsF_6$ 0.50 M in acetonitrile and for the systems $LiAsF_6$ 0.5 M + poly(ethylene oxide) polymers of average molar masses 400, 1000, and 2000 respectively in acetonitrile. The composition of these mixtures corresponds to a molar ratio $R = [(-CH_2-CH_2-O-)]/[Li^+] = 4$. Except for the system

tetraglyme 0.5 M + $LiAsF_6$ 0.5 M, the spectral envelopes have been deconvoluted by three Gaussian-Lorentzian product functions.

Table IV (microfilm edition) reports also the parameters related to the IR spectra of the polyethers alone in CH_3CN at the same concentrations as studied for the systems containing $LiAsF_6$ and in the 910-780 cm^{-1} range. Three Gaussian-Lorentzian product functions suffice to describe the spectral profiles.

Figure 13 reports the most salient information from the above spectra, namely the decrease in the normalized absorbance for the band appearing in the range 860-880 cm^{-1} (for the various systems investigated) vs. the molar mass $\bar{M}$ of the polyethers. The rapid decrease in (A_2^o/ℓ) with $\bar{M}$, when Li^+ is present, resembles the behavior of μ_{II} as a function of $\bar{M}$ (Fig. 12). It is possible that both μ_{II} and A_2^o/ℓ reflect the increasing difficulty, by increasing $\bar{M}$, of forming a given coordinated structure around Li^+. This would cause a decrease in absorbance and in μ_{II} (through ΔV_{II}) for the IR band and ultrasonic spectrum, respectively.

The other main relevant feature of the IR spectra is the appearance of a new band for $LiAsF_6$ 0.5 M + tetraglyme 0.5 M in acetonitrile at $\bar{\nu}^o$ = 837 cm^{-1} (termed arbitrarily $\bar{\nu}_4^o$). The new band is sizeable (Fig. 14); its absorbance is comparable to the band at $\bar{\nu}_3^o$ = 869 cm^{-1}, which is the one

enhanced by Li^+ when added to the polyethers (Fig. 13). It is possible that for tetraglyme, as the oxygen to Li^+ ratio is 5 instead of 4 (as for the other systems) a different coordination symmetry is being formed.

Acknowledgments

The authors wish to express gratitude to the National Science Foundation, to the Joint Service Program of Polytechnic University and to the Office of Naval Research for support of various aspects of this work.

References

1. Eyring, E.M.; Petrucci, S., in Cation Binding by Macrocycles, edited by Inoue, Y. and Gokel, G.W., Marcel Dekker, New York, in press.

2. Eigen, M.; Winkler R., in Neurosciences, Second Study Program, Schmit, F.O. Editor, Rockefeller Univ. Press, New York (1970), page 685.

3. Cabbiness, D.K.; Margerum, D.W., J. Am. Chem. Soc. (1969) 91, 6540.

4. For a review see Farber, H.; Petrucci, S., in The Chemical Physics of Solvation, part B, Chapter 9, "Ultrasonic Absorption Spectrometry", edited by Dogonadze, R. R. et al., Elsevier, Amsterdam (1986).

5. Sato, H.; Kusumoto, Y., Chem. Letters (1978) 635.

6. For a review see Zundel, G.; Fritsch, J., in The Chemical Physics of Solvation, part B, Chapter 2, "Interaction in and Structure of Ionic Solutions and Polyelectrolytes-Infrared Results," page 53, edited by Dogonadze, R.R. et al., Elsevier, Amsterdam (1986).

7. Saar, D.; Petrucci, S., J. Phys. Chem. (1986) 90, 3326.

8. Eigen, M.; Tamm, K., Z. Elektrochem. (1962) 66, 93, 107; Tamm, K. in Dispersion and Absorption of Sound by Molecular Processes, D. Sette, Editor, Academic Press, New York (1963).

9. For a discussion of this function see Maaser, H.; Xu, M.; Hemmes, P.; Petrucci, S., J. Phys. Chem. (1987) 91, 3047; Inoue, N.; Xu, M.; Petrucci, S., J. Phys. Chem. (1987) 91, 4628.

Glossary of Figures

Fig. 1 A. Representative ultrasonic spectrum in the form of excess ultrasonic absorption per wavelength μ *vs.* the frequency f for $LiClO_4$ + Triglyme at R = 1 in acetonitrile at 25°C.

B. Representative ultrasonic spectrum in the form μ *vs.* f for $LiClO_4$ + PEO at an oxygen to Li^+ molar ratio R_{PEO} = 4 in acetonitrile at 25°C.

Fig. 2 A. Values of the sound velocity u *vs.* concentration of electrolyte C for all systems investigated in acetonitrile at 25°C.

B. Value of the ratio $B = \left(\frac{\alpha}{f^2}\right)_{f>>f_I,f_{II}}$ *vs.* concentration C for all the systems investigated in acetonitrile at 25°C.

Fig. 3 A. Inverse of the relaxation time of the "fast" process τ_I^{-1} *vs.* the concentration of electrolyte for all the systems investigated in acetonitrile at 25°C.

B. Inverse of the relaxation time of the "slow" process τ_{II}^{-1} *vs.* the concentration of electrolyte for all the systems investigated in acetonitrile at 25°C.

Fig. 4 A. Excess sound absorption coefficient for wavelength μ_I for the "fast" process *vs.* concentration of electrolyte for all the systems investigated in CH_3CN at 25°C.

B. Plot of μ_{II} for the "slow" process vs. C for all the systems investigated in CH_3CN at 25°C.

Fig. 5 A. Plot of μ_I vs. Γ_I^{-1} for $LiCl\ell O_4$ + PEO at molar ratio R = 4 and C $\leq$ 0.5 M in acetonitrile at 25°C.

B. Plot of μ_{II} vs. Γ_{II}^{-1} for $LiCl\ell O_4$ + PEO at R = 4.0 and C $\leq$ 0.32 M in acetonitrile at 25°C.

Fig. 6 A. Digitized infrared spectrum [Absorbance vs. $\bar{\nu}$ (cm^{-1})] of triglyme 0.6 M in acetonitrile in the 800-900 cm^{-1} region.

B. Digitized absorbances vs. wavenumber for $LiCl\ell O_4$ 0.6 M + Triglyme 0.6 M in acetonitrile in the 800-900 cm^{-1} region.

C. Digitized absorbance vs. wavenumber for $LiAsF_6$ 0.6 M + Triglyme 0.6 M in acetonitrile in the 800-900 cm^{-1} region.

Fig. 7. A. Normalized absorbances per unit cell length A_J^o/ℓ vs. concentration for the deconvoluted spectrum (expressed by the three bands) of triglyme in CH_3CN.

B. Normalized absorbance per unit cell length A_J^o/ℓ vs. concentration for $LiCl\ell O_4$ or $LiAsF_6$ + Triglyme at R = 1 in acetonitrile.

Fig. 8. A. Digitized infrared spectrum in the 800-900 cm^{-1} region for PEO of molar unit $(-CH_2-CH_2-O-)_4$ 0.4 M in acetonitrile.

B. Digitized infrared spectrum in the 800-900 cm^{-1} region for $LiCl O_4$ + PEO at molar ratio R [oxygen]/$[Li^+]$ = 4 in acetonitrile.

C. Digitized infrared spectrum in the 800-900 cm^{-1} region for $LiAsF_6$ + PEO at molar ratio R [oxygen]/$[Li^+]$ = 4 in acetonitrile.

Fig. 9 A,B,C Normalized absorbances A_j^o/ℓ per unit cell length of the three bands of PEO and of PEO + Lithium salts in acetonitrile.

Fig. 10 A. Ultrasonic spectrum of $LiCl O_4$ 0.3 M + 12C4 0.3 M in acetonitrile at 25° C.

B. Representative digitized spectrum of 12C4 in acetonitrile in the 800-900 cm^{-1} region.

C. Representative digitized spectrum of $LiCl O_4$ + 12C4 at R = $\frac{[12C4]}{[LiCl O_4]}$ = 0.5 in acetonitrile in the 800-900 cm^{-1} region.

Fig. 11 A. Normalized absorbance A_j^o/ℓ <u>vs</u>. concentration for the 12C4 in acetonitrile.

B. Normalized absorbance A_j^o/ℓ *vs.* concentration for $LiCl\ell O_4$ + 12C4 at R = 0.5 in acetonitrile.

Fig. 12 Dependence of μ_I and of μ_{II} on the average molar mass $\bar{M}$ of the polyether for $LiAsF_6$ 0.5 M + polyether in acetonitrile.

Fig. 13 Dependence of the normalized absorbance A_3^o/ℓ upon average molar mass $\bar{M}$ of the polyether for $LiAsF_6$ + polyethers and for polyethers in acetonitrile.

Fig. 14 Deconvoluted infrared spectral envelope of the digitized spectrum of the system $LiAsF_6$ 0.50 M + tetraglyme 0.50 M in CH_3CN. The dashed Gaussian-Lorentzian component centered at ν^o = 837 cm^{-1} is specific for the tetraglyme + Li^+ solution.

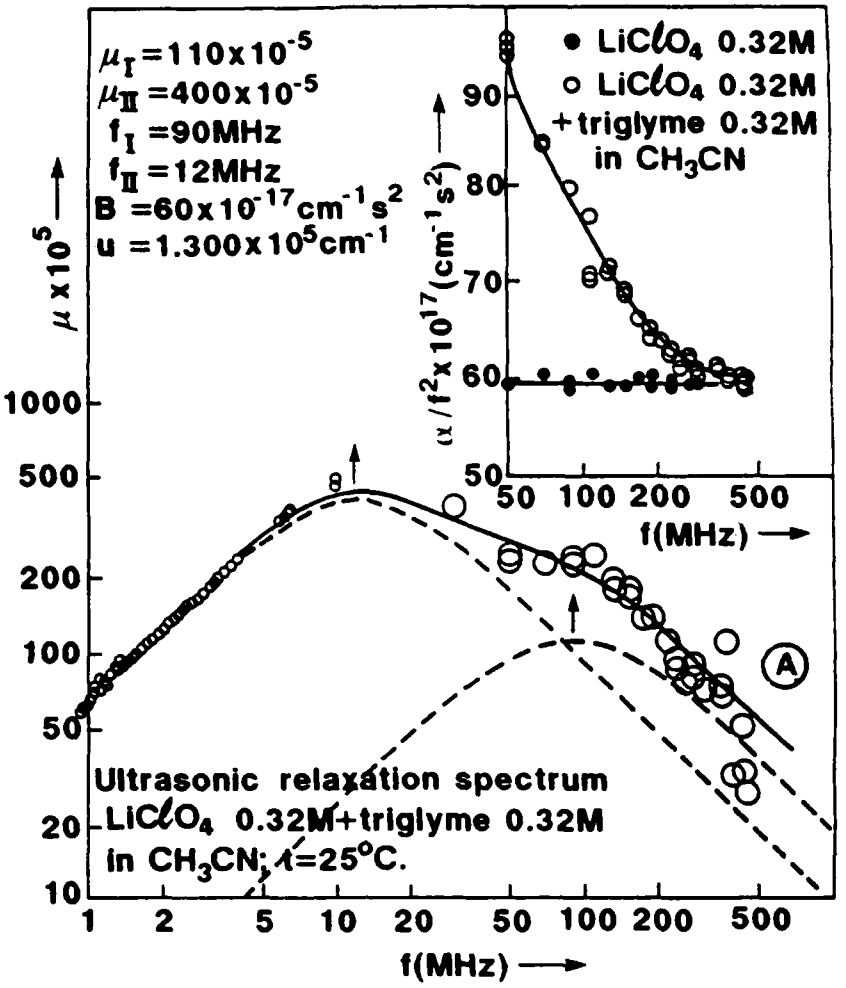
$\mu_I = 110 \times 10^{-5}$
$\mu_{II} = 400 \times 10^{-5}$
$f_I = 90MHz$
$f_{II} = 12MHz$
$B = 60 \times 10^{-17} cm^{-1} s^2$
$u = 1.300 \times 10^5 cm^{-1}$
$\mu \times 10^5$
f(MHz)
• $LiClO_4$ 0.32M
○ $LiClO_4$ 0.32M +triglyme 0.32M in CH_3CN
$\alpha / f^2 \times 10^{17} (cm^{-1} s^2)$
A
Ultrasonic relaxation spectrum
$LiClO_4$ 0.32M+triglyme 0.32M
in CH_3CN; t=25°C.

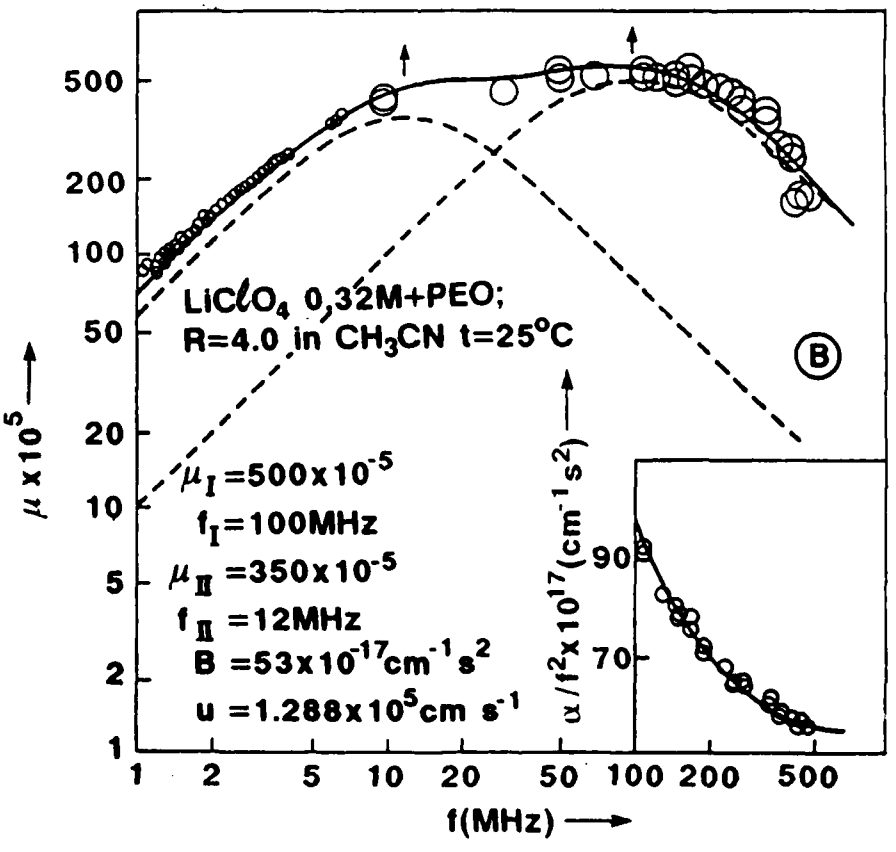
$LiClO_4$ 0,32M+PEO;
R=4.0 in CH_3CN t=25°C
B
$\mu_I = 500 \times 10^{-5}$
$f_I = 100MHz$
$\mu_{II} = 350 \times 10^{-5}$
$f_{II} = 12MHz$
$B = 53 \times 10^{-17} cm^{-1} s^2$
$u = 1.288 \times 10^5 cm\ s^{-1}$
$\mu \times 10^5$
f(MHz)
$\alpha / f^2 \times 10^{17} (cm^{-1} s^2)$

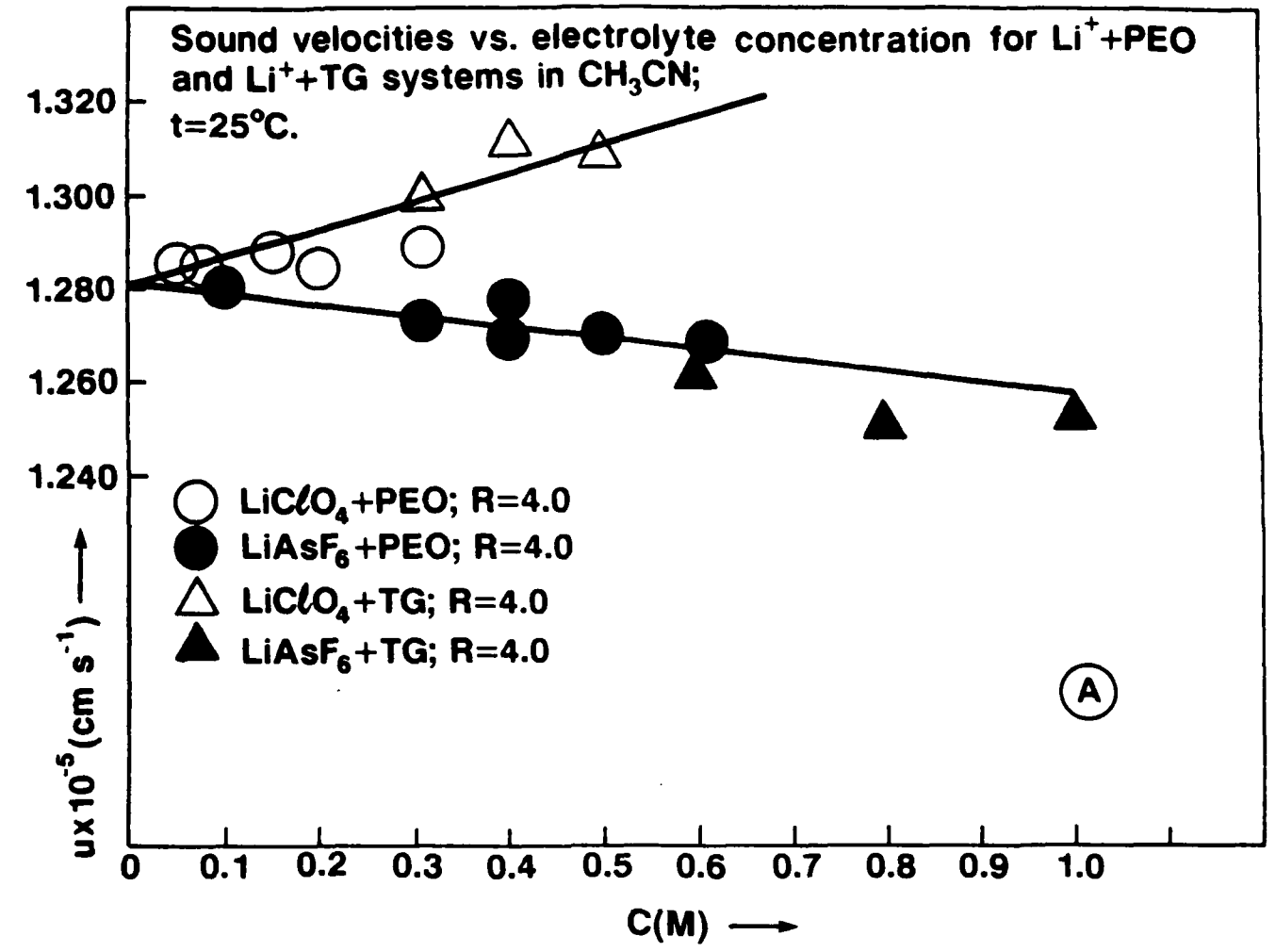
Sound velocities vs. electrolyte concentration for Li+ +PEO and Li+ +TG systems in CH3CN;
t=25°C.
1.320
1.300
1.280
1.260
1.240
LiClO4+PEO; R=4.0
LiAsF6+PEO; R=4.0
LiClO4+TG; R=4.0
LiAsF6+TG; R=4.0
A
ux10-5 (cm s-1)
0
0.1
0.2
0.3
0.4
0.5
0.6
0.7
0.8
0.9
1.0
C(M)

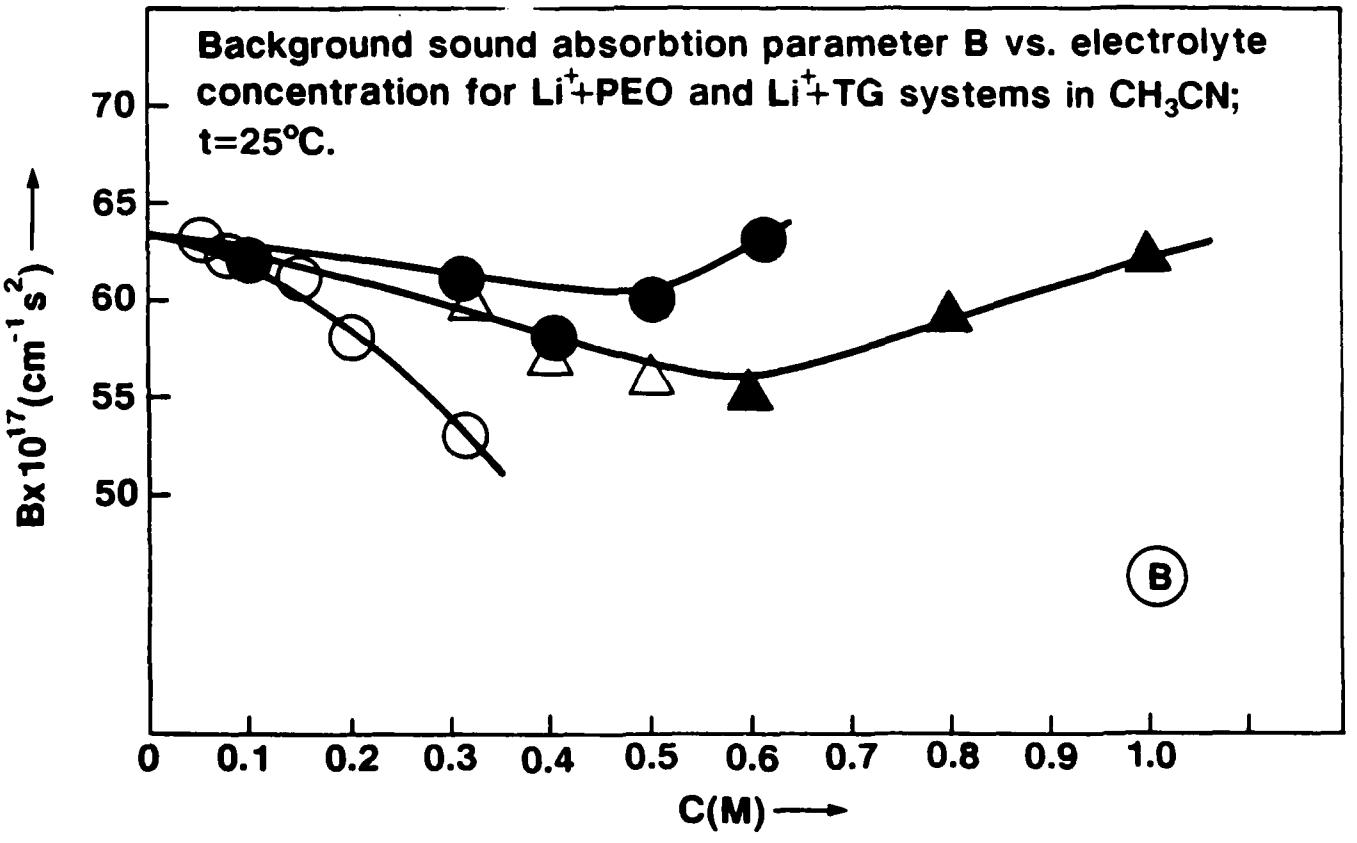
Background sound absorbtion parameter B vs. electrolyte concentration for Li+ +PEO and Li+ +TG systems in CH3CN;
t=25°C.
70
65
60
55
50
B
Bx10^17 (cm^-1 s^2)
0
0.1
0.2
0.3
0.4
0.5
0.6
0.7
0.8
0.9
1.0
C(M)

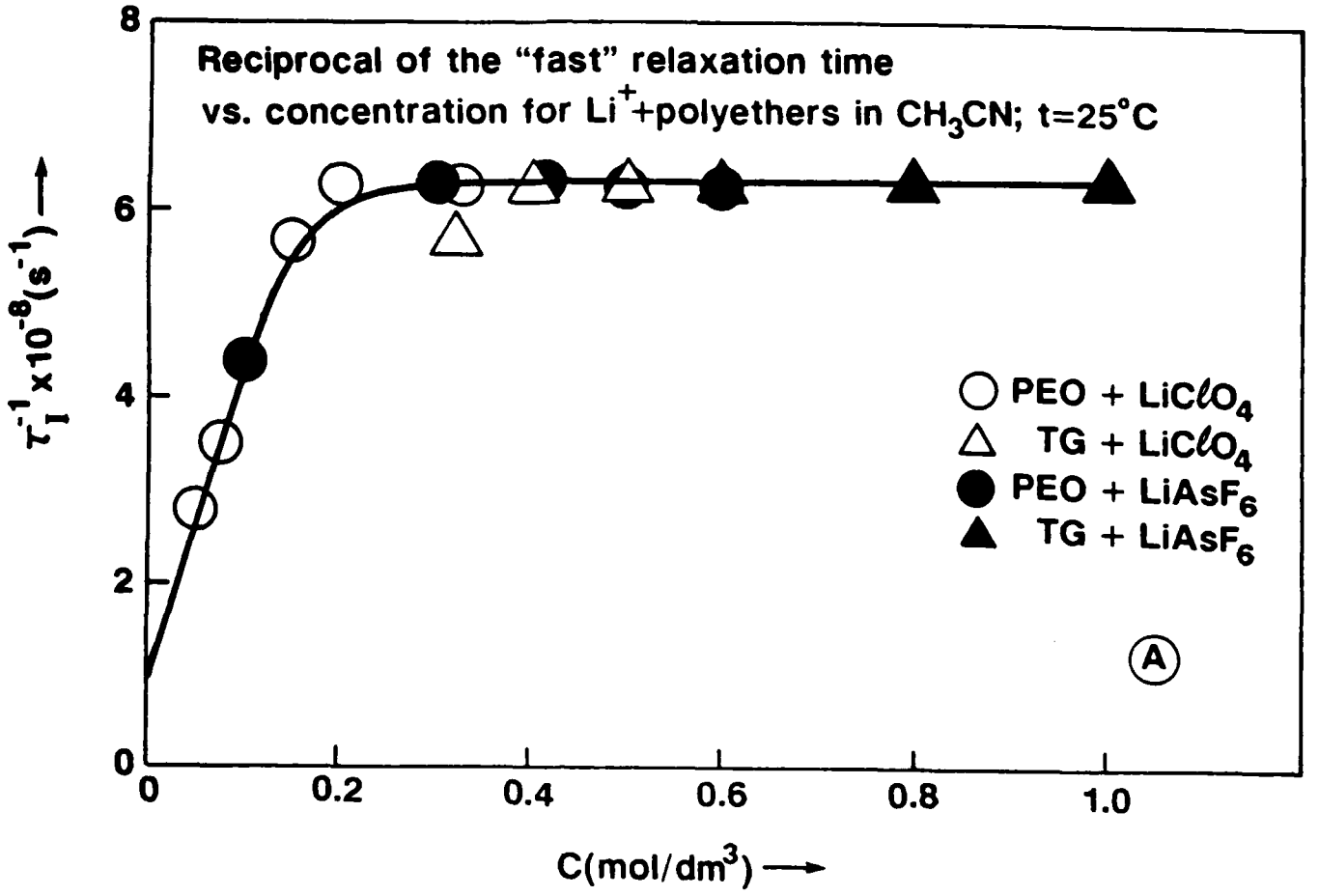
Reciprocal of the "fast" relaxation time
vs. concentration for Li+ +polyethers in CH3CN; t=25°C
τI-1 x10-8(s-1) →
C(mol/dm3) →
PEO + LiClO4
TG + LiClO4
PEO + LiAsF6
TG + LiAsF6
A
0
2
4
6
8
0.2
0.4
0.6
0.8
1.0

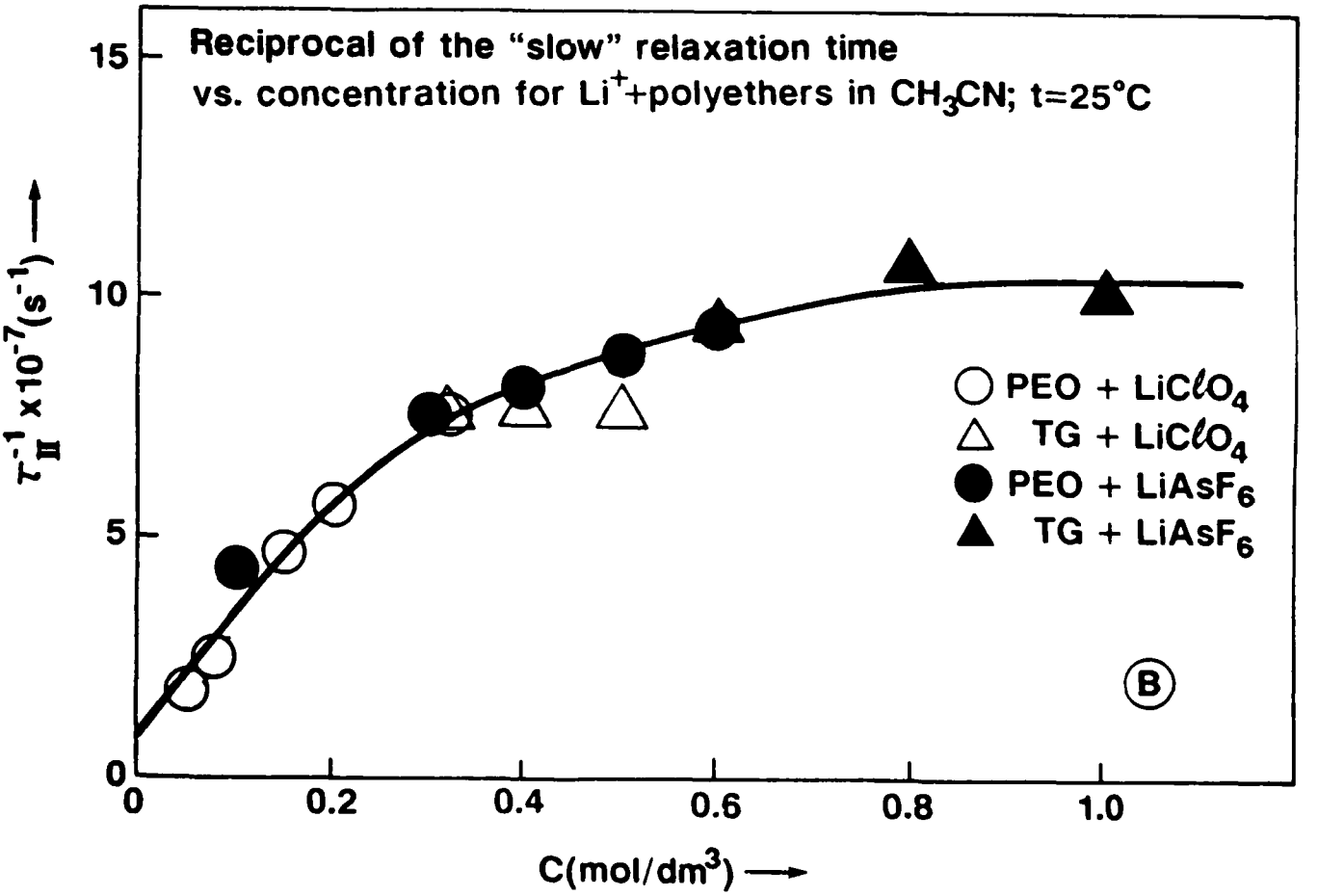
Reciprocal of the "slow" relaxation time
vs. concentration for Li+ +polyethers in CH3CN; t=25°C
τII-1 x10-7(s-1) →
C(mol/dm3) →
PEO + LiClO4
TG + LiClO4
PEO + LiAsF6
TG + LiAsF6
B
0
5
10
15
0.2
0.4
0.6
0.8
1.0

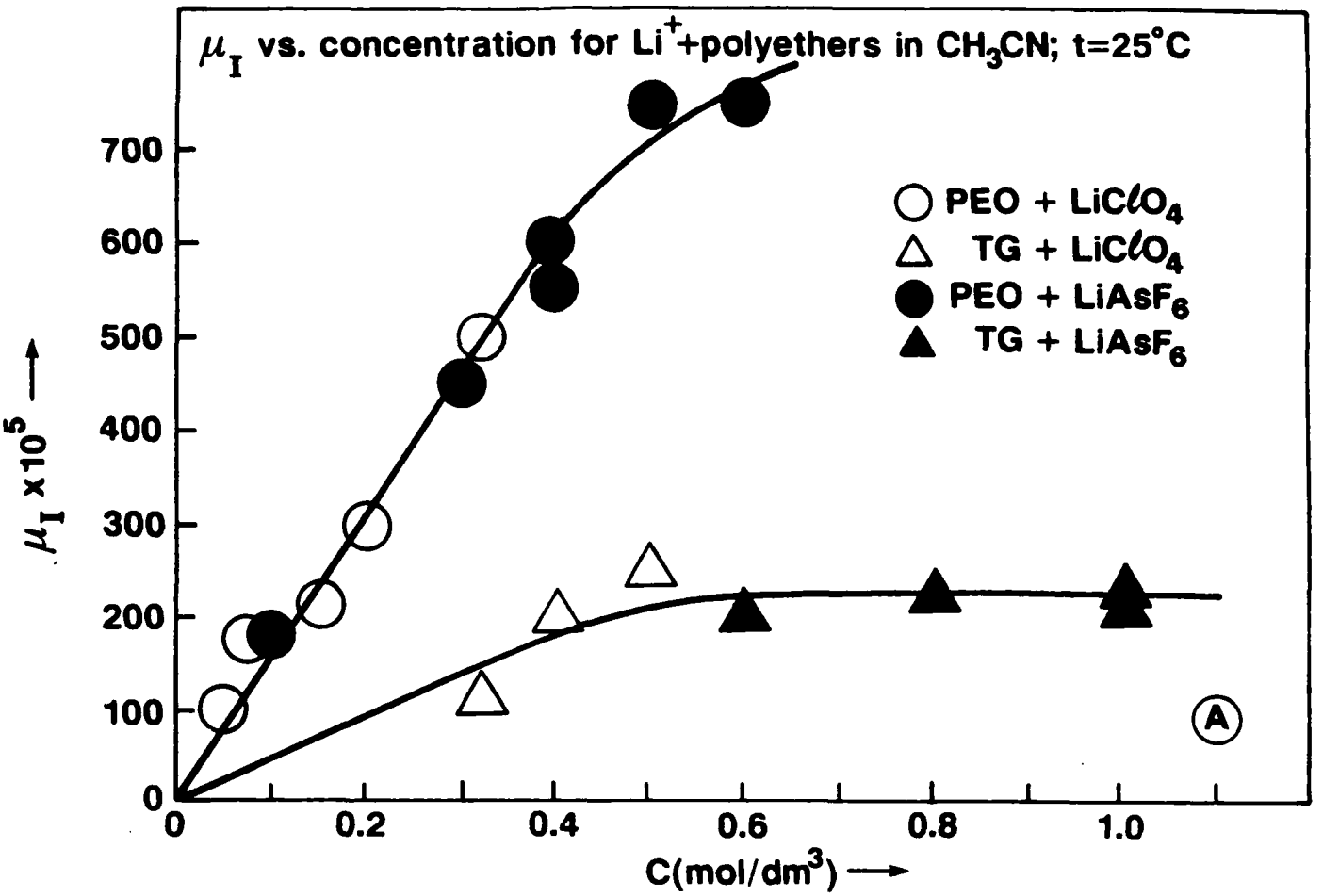
μ_I vs. concentration for Li^++polyethers in CH_3CN; t=25°C
$\mu_I \times 10^5$ ⟶
C(mol/dm^3) ⟶
PEO + $LiClO_4$
TG + $LiClO_4$
PEO + $LiAsF_6$
TG + $LiAsF_6$
A
0
100
200
300
400
500
600
700
0.2
0.4
0.6
0.8
1.0

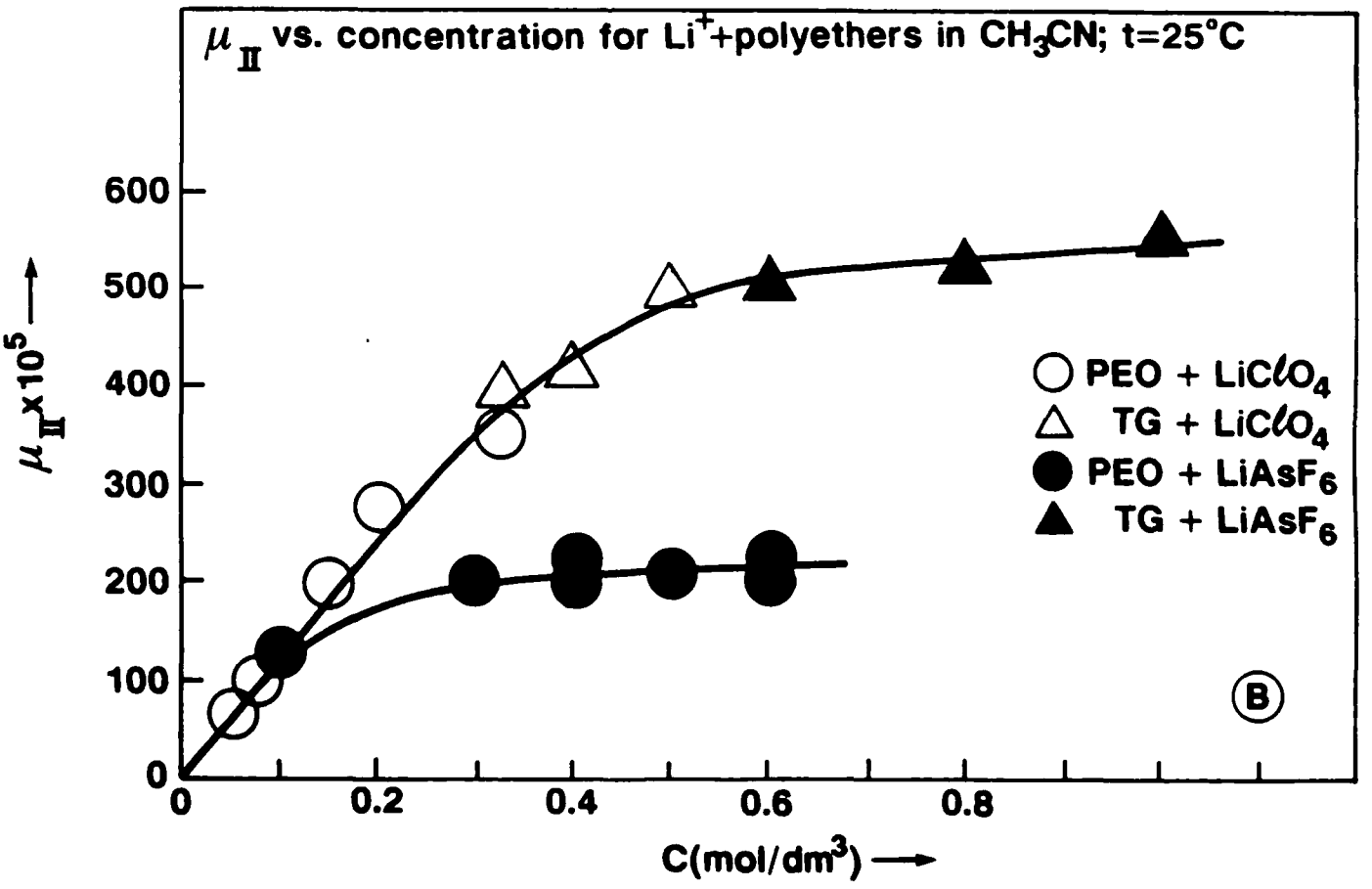
μ_{II} vs. concentration for Li^++polyethers in CH_3CN; t=25°C
$\mu_{II} \times 10^5$ ⟶
C(mol/dm^3) ⟶
PEO + $LiClO_4$
TG + $LiClO_4$
PEO + $LiAsF_6$
TG + $LiAsF_6$
B
0
100
200
300
400
500
600
0.2
0.4
0.6
0.8

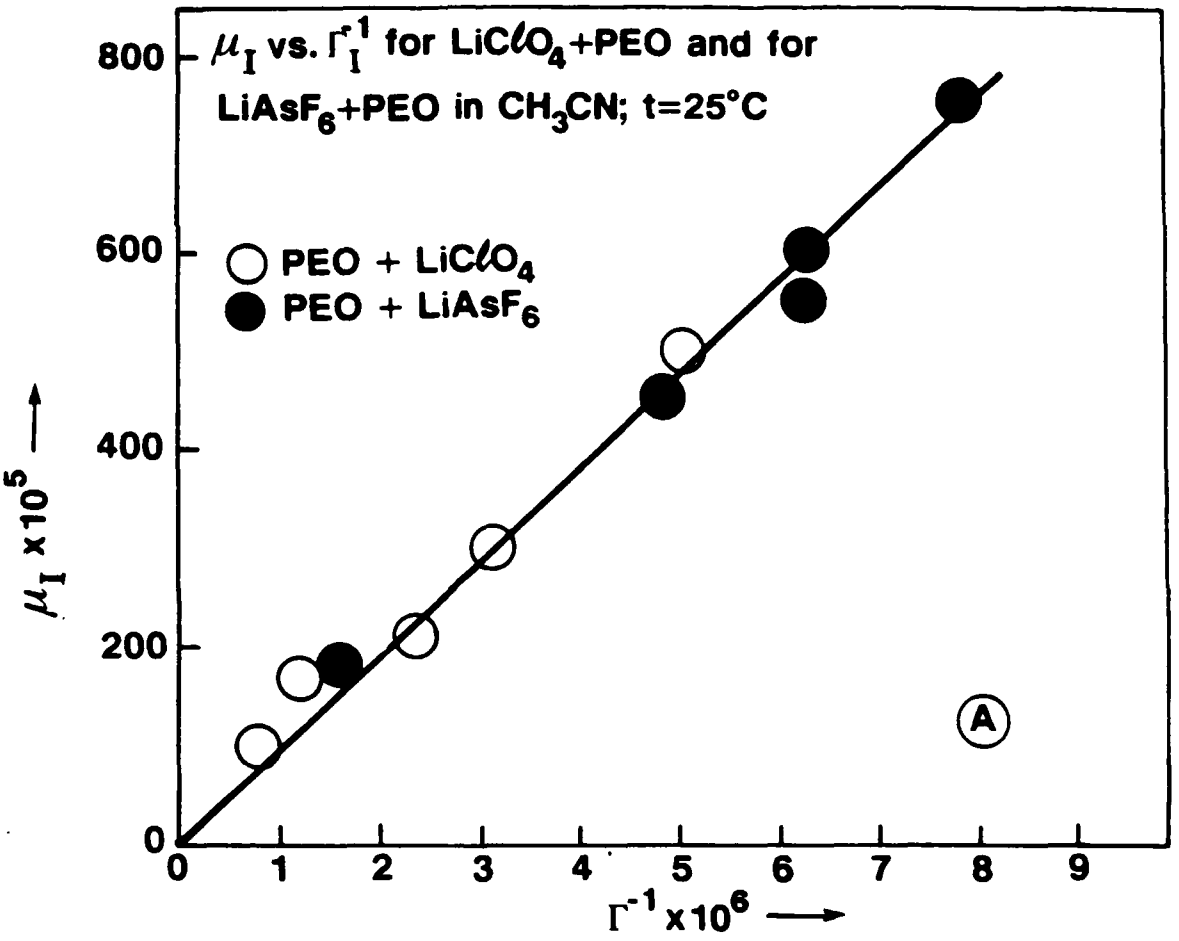
μ_I vs. Γ_I^{-1} for $LiClO_4$+PEO and for
$LiAsF_6$+PEO in CH_3CN; t=25°C
PEO + $LiClO_4$
PEO + $LiAsF_6$
$\mu_I \times 10^5$
$\Gamma^{-1} \times 10^6$
A

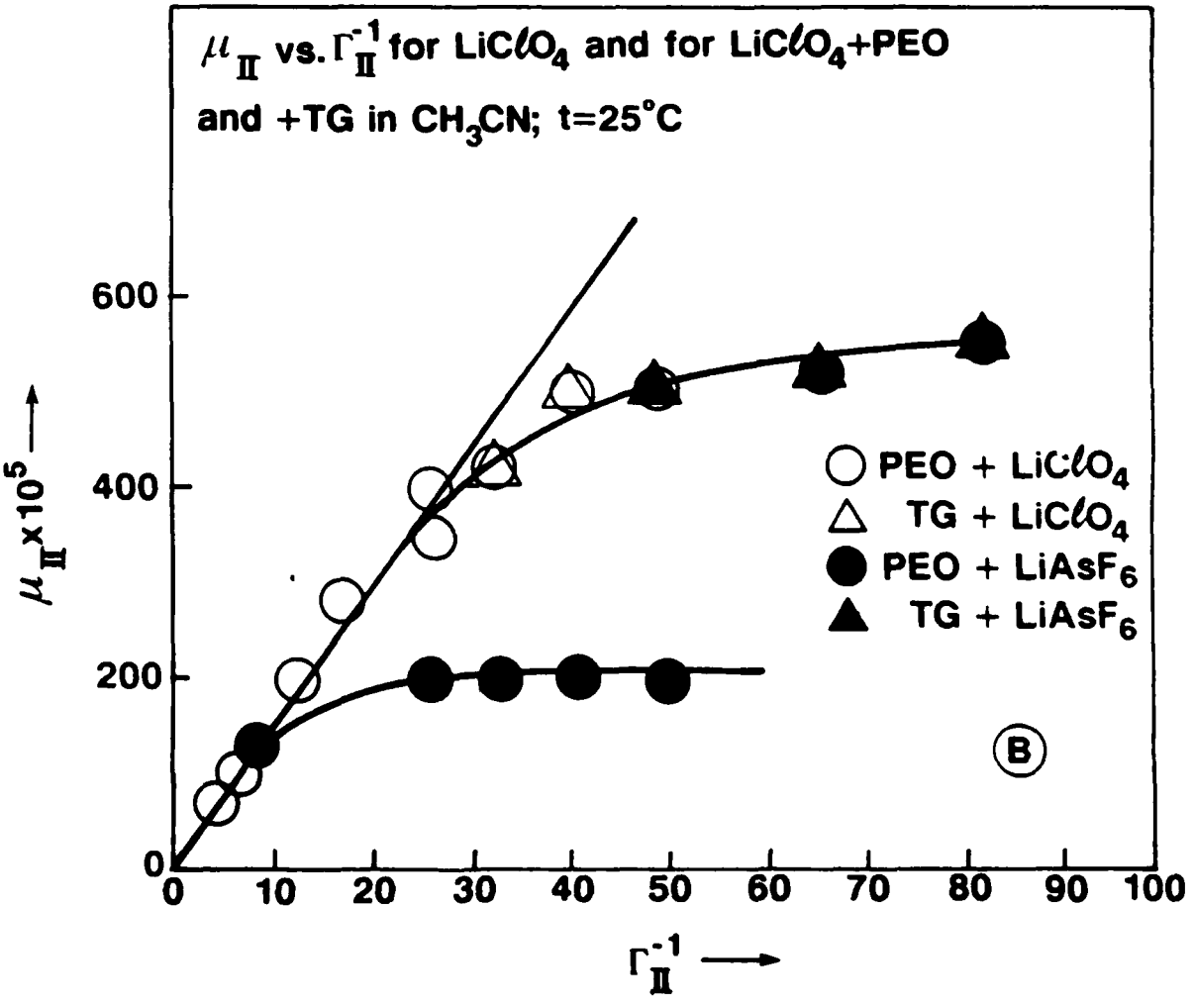
μ_{II} vs. Γ_{II}^{-1} for $LiClO_4$ and for $LiClO_4$+PEO
and +TG in CH_3CN; t=25°C
PEO + $LiClO_4$
TG + $LiClO_4$
PEO + $LiAsF_6$
TG + $LiAsF_6$
$\mu_{II} \times 10^5$
Γ_{II}^{-1}
B

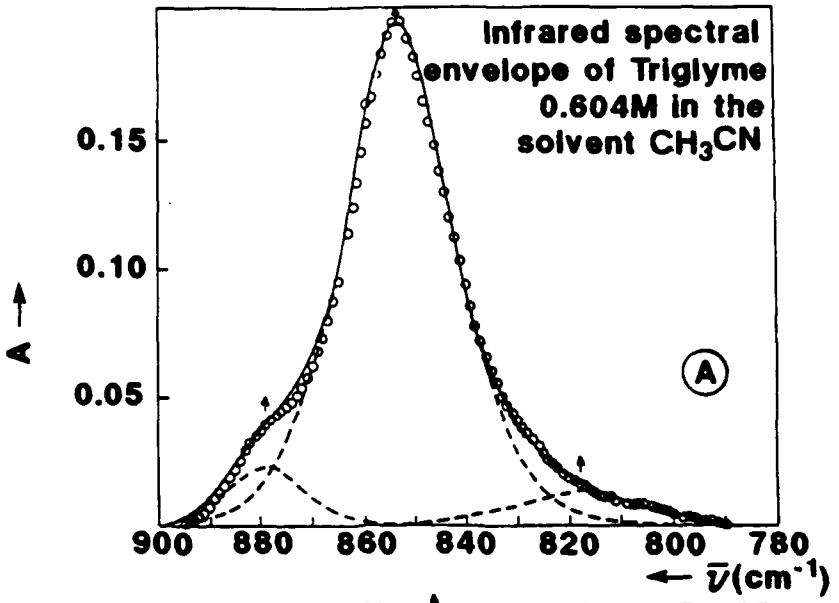
Infrared spectral
envelope of Triglyme
0.604M in the
solvent CH_3CN
A
0.15
0.10
0.05
900 880 860 840 820 800 780
$\leftarrow \bar{\nu}(cm^{-1})$

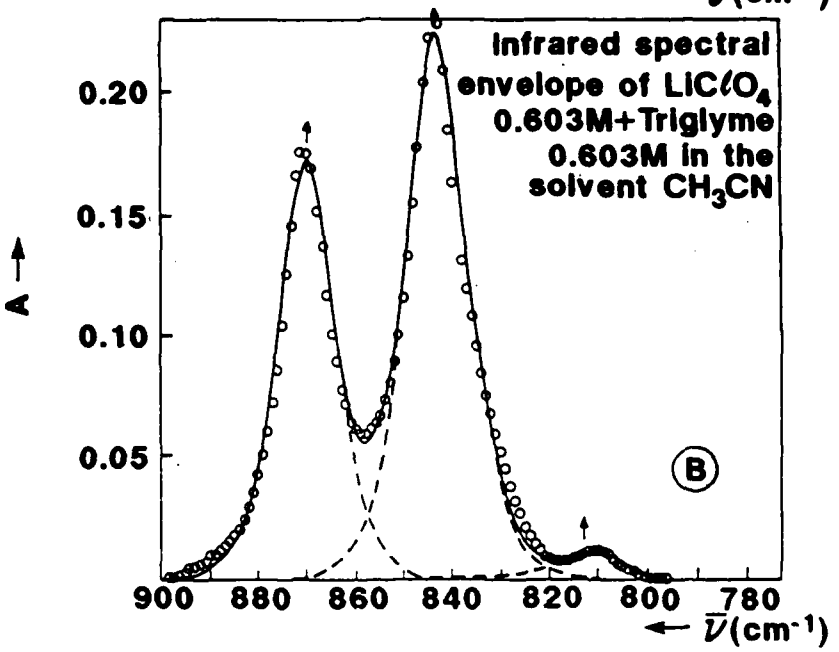
Infrared spectral
envelope of $LiClO_4$
0.603M+Triglyme
0.603M in the
solvent CH_3CN
B
0.20
0.15
0.10
0.05
900 880 860 840 820 800 780
$\leftarrow \bar{\nu}(cm^{-1})$

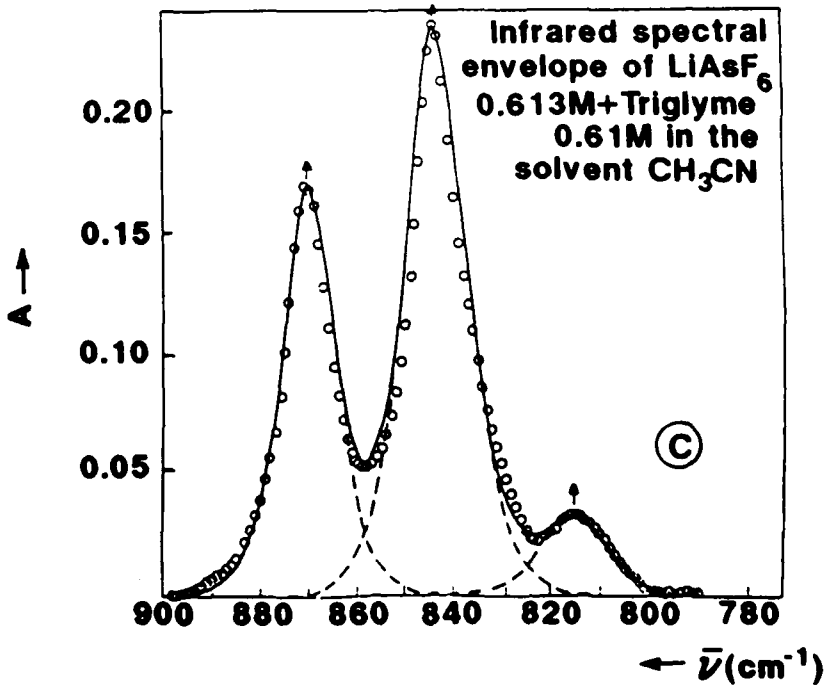
Infrared spectral
envelope of $LiAsF_6$
0.613M+Triglyme
0.61M in the
solvent CH_3CN
C
0.20
0.15
0.10
0.05
900 880 860 840 820 800 780
$\leftarrow \bar{\nu}(cm^{-1})$

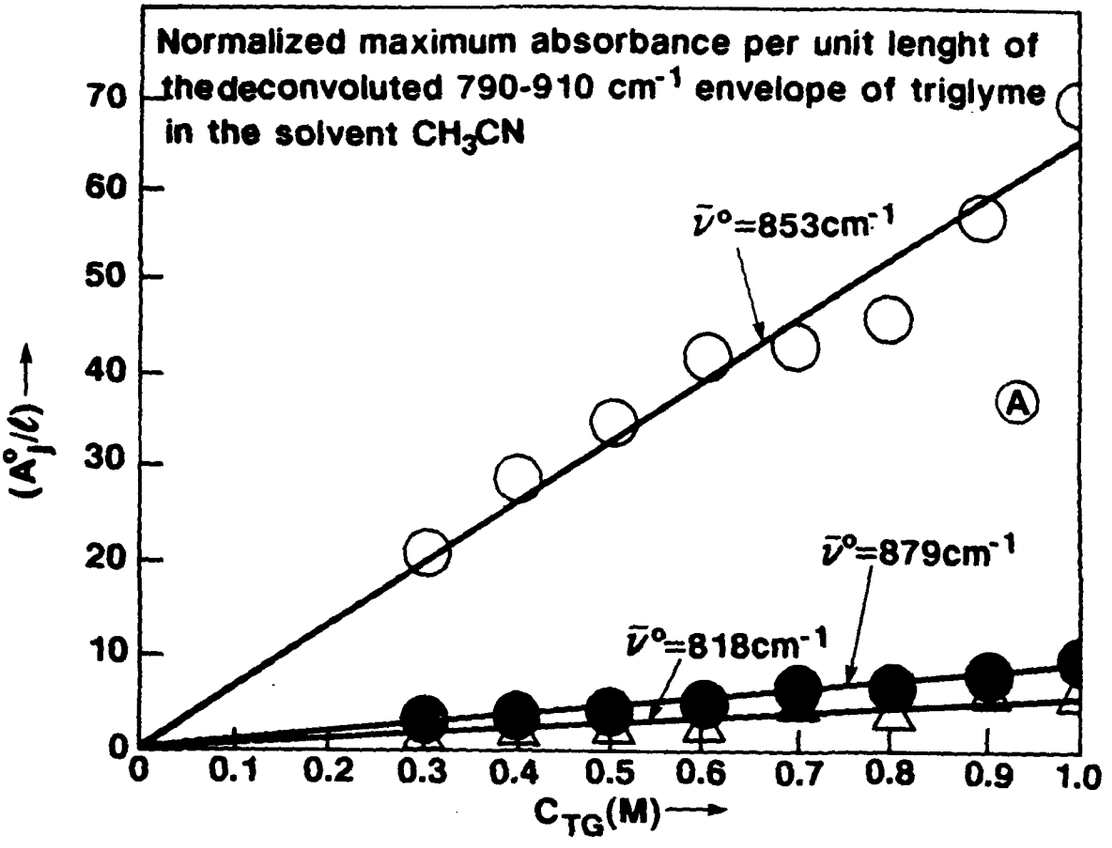
Normalized maximum absorbance per unit lenght of thedeconvoluted 790-910 cm-1 envelope of triglyme in the solvent CH3CN
ν̄°=853cm-1
ν̄°=879cm-1
ν̄°=818cm-1
A
(Aj°/ℓ) ⟶
CTG(M) ⟶
0
10
20
30
40
50
60
70
0.1
0.2
0.3
0.4
0.5
0.6
0.7
0.8
0.9
1.0

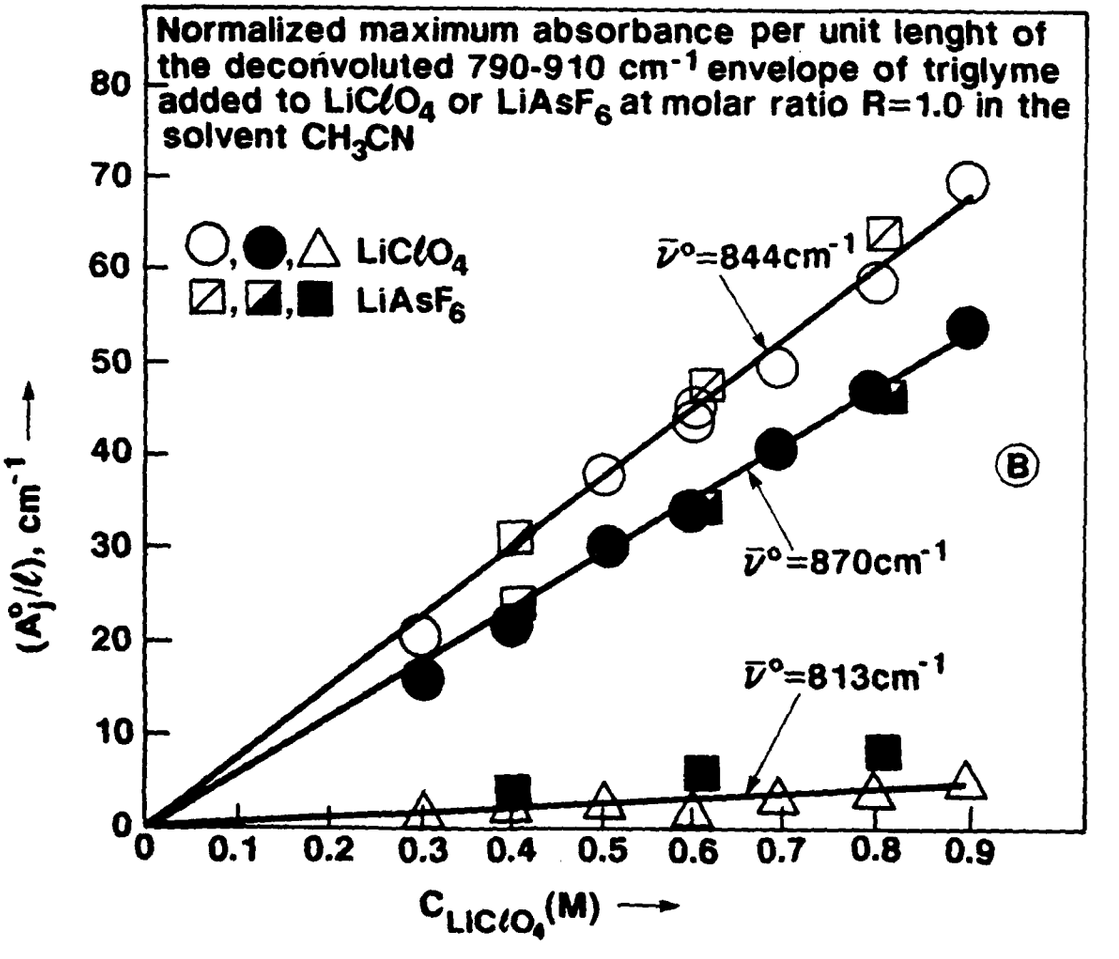
Normalized maximum absorbance per unit lenght of the deconvoluted 790-910 cm-1 envelope of triglyme added to LiClO4 or LiAsF6 at molar ratio R=1.0 in the solvent CH3CN
○,●,△ LiClO4
□,◪,■ LiAsF6
ν̄°=844cm-1
ν̄°=870cm-1
ν̄°=813cm-1
B
(Aj°/ℓ), cm-1 ⟶
CLiClO4(M) ⟶
0
10
20
30
40
50
60
70
80
0.1
0.2
0.3
0.4
0.5
0.6
0.7
0.8
0.9

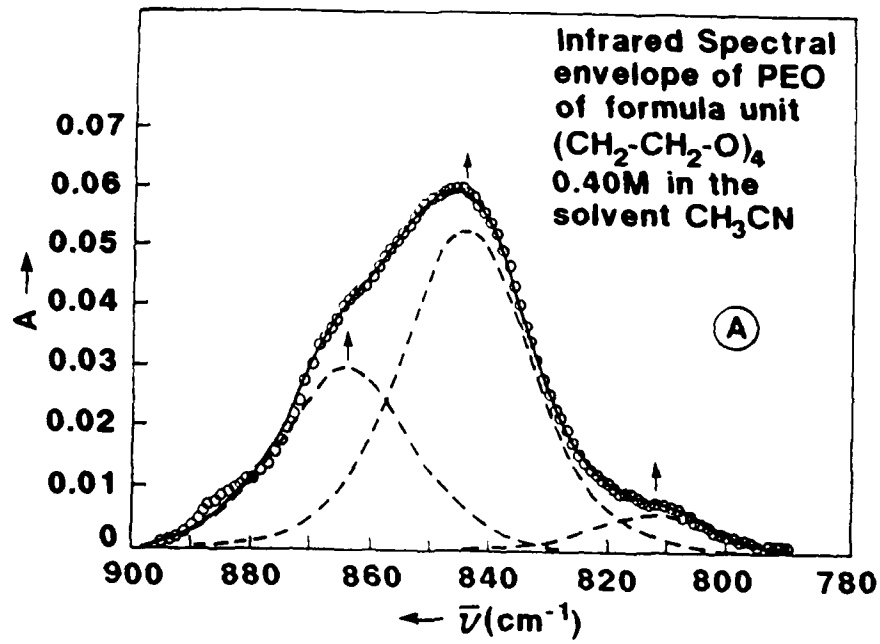
Infrared Spectral envelope of PEO of formula unit $(CH_2-CH_2-O)_4$ 0.40M in the solvent CH_3CN
A
0.07
0.06
0.05
0.04
0.03
0.02
0.01
0
900 880 860 840 820 800 780
$\bar{\nu}(cm^{-1})$

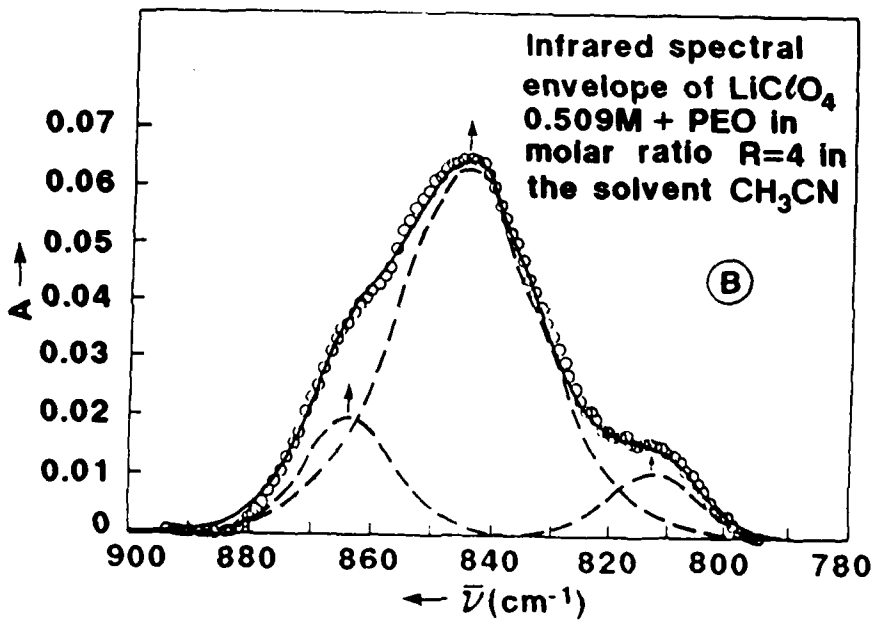
Infrared spectral envelope of $LiC\ell O_4$ 0.509M + PEO in molar ratio R=4 in the solvent CH_3CN
B
A
0.07
0.06
0.05
0.04
0.03
0.02
0.01
0
900 880 860 840 820 800 780
$\bar{\nu}(cm^{-1})$

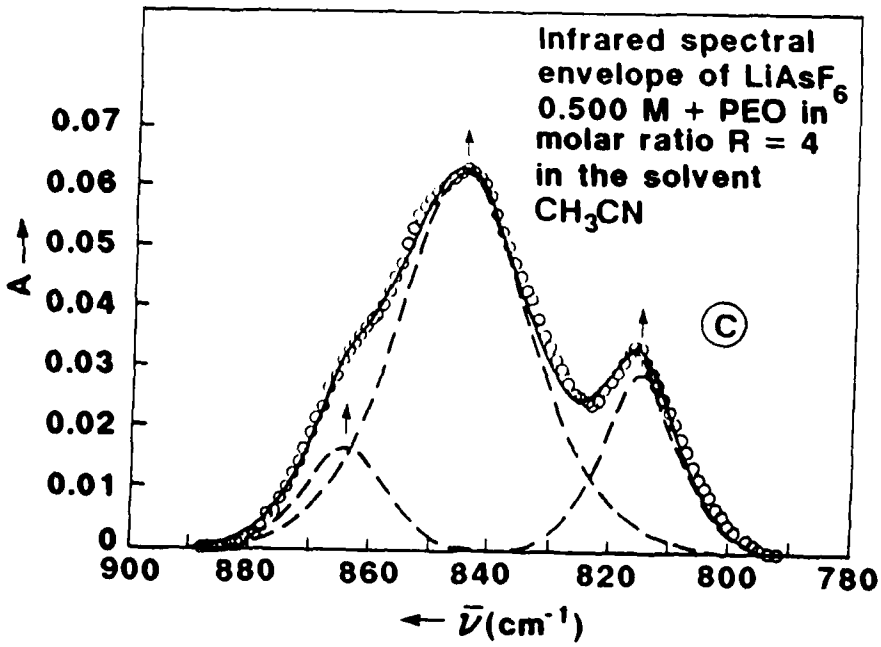
Infrared spectral envelope of $LiAsF_6$ 0.500 M + PEO in molar ratio R = 4 in the solvent CH_3CN
C
A
0.07
0.06
0.05
0.04
0.03
0.02
0.01
0
900 880 860 840 820 800 780
$\bar{\nu}(cm^{-1})$

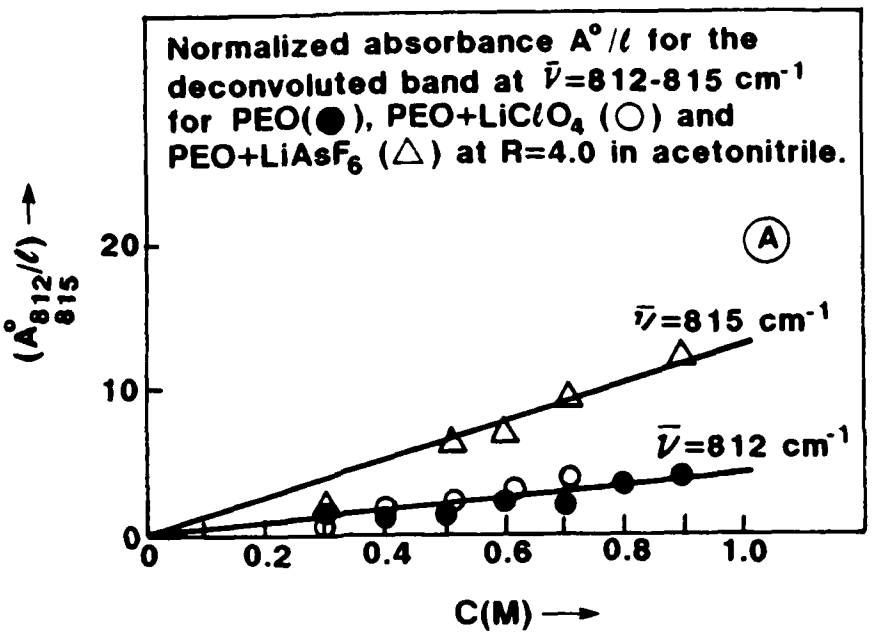
Normalized absorbance A°/ℓ for the deconvoluted band at $\bar{\nu}$=812-815 cm^{-1} for PEO(●), PEO+LiCℓO$_4$ (○) and PEO+LiAsF$_6$ (△) at R=4.0 in acetonitrile.
A
$\bar{\nu}$=815 cm^{-1}
$\bar{\nu}$=812 cm^{-1}
$(A^{\circ}_{812-815}/\ell)$ →
0
10
20
0
0.2
0.4
0.6
0.8
1.0
C(M) →

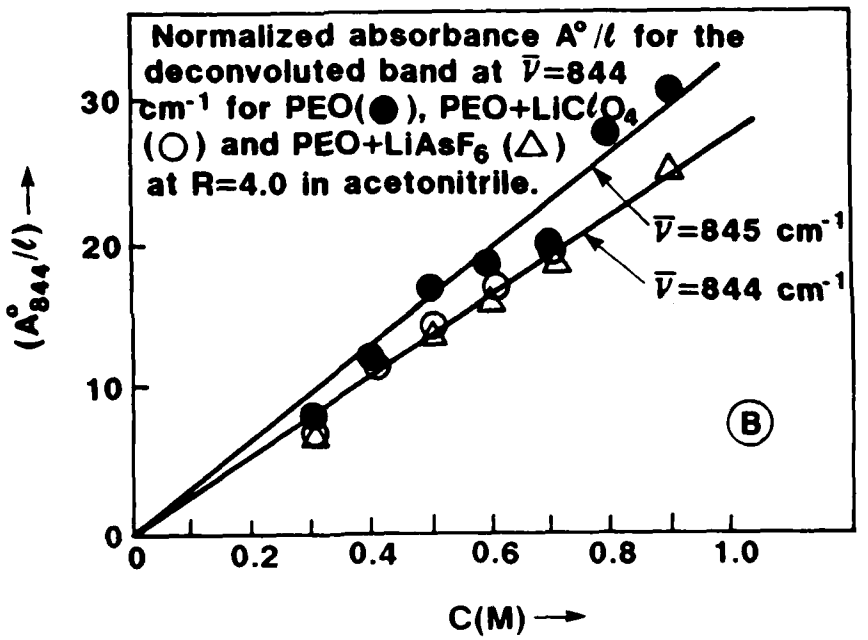
Normalized absorbance A°/ℓ for the deconvoluted band at $\bar{\nu}$=844 cm^{-1} for PEO(●), PEO+LiCℓO$_4$ (○) and PEO+LiAsF$_6$ (△) at R=4.0 in acetonitrile.
$\bar{\nu}$=845 cm^{-1}
$\bar{\nu}$=844 cm^{-1}
B
(A°_{844}/ℓ) →
0
10
20
30
0
0.2
0.4
0.6
0.8
1.0
C(M) →

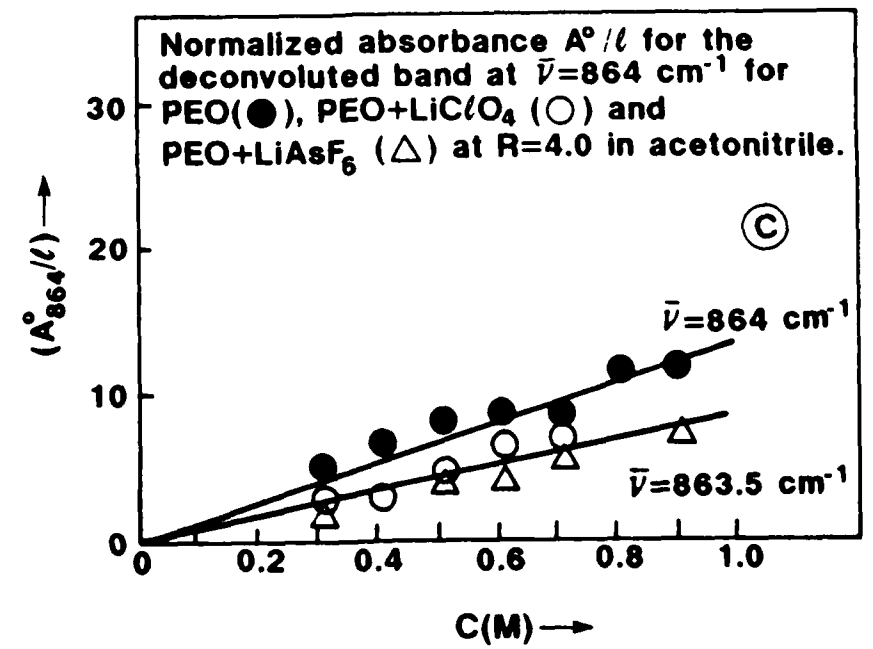
Normalized absorbance A°/ℓ for the deconvoluted band at $\bar{\nu}$=864 cm^{-1} for PEO(●), PEO+LiCℓO$_4$ (○) and PEO+LiAsF$_6$ (△) at R=4.0 in acetonitrile.
C
$\bar{\nu}$=864 cm^{-1}
$\bar{\nu}$=863.5 cm^{-1}
(A°_{864}/ℓ) →
0
10
20
30
0
0.2
0.4
0.6
0.8
1.0
C(M) →

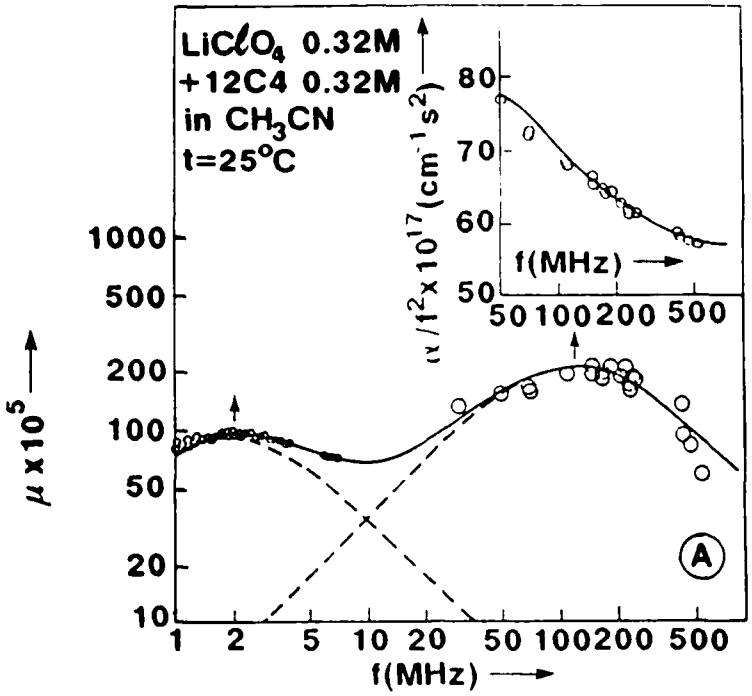
LiClO4 0.32M
+12C4 0.32M
in CH3CN
t=25°C
μ x10^5
f(MHz)
A

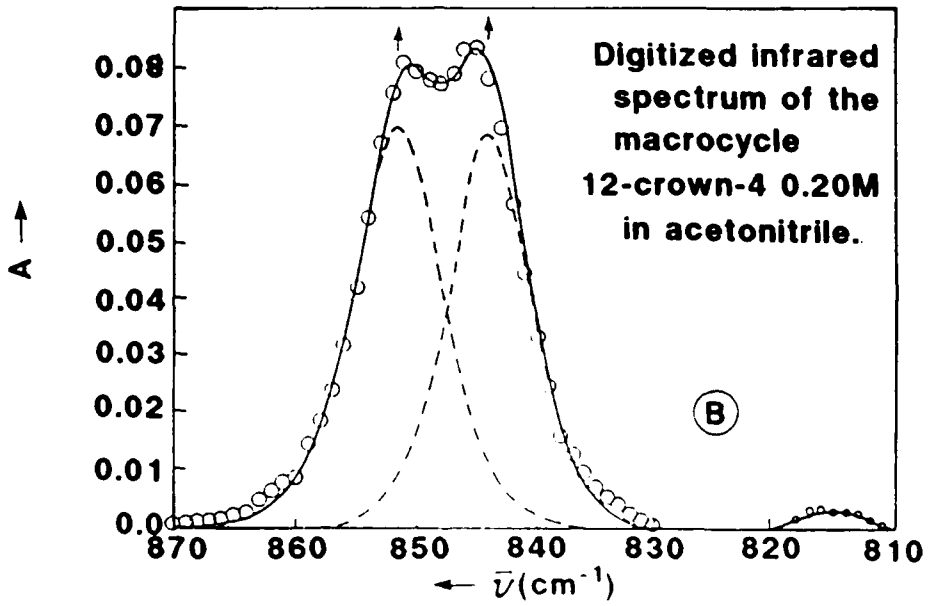
Digitized infrared
spectrum of the
macrocycle
12-crown-4 0.20M
in acetonitrile.
A
B
ν̄(cm⁻¹)

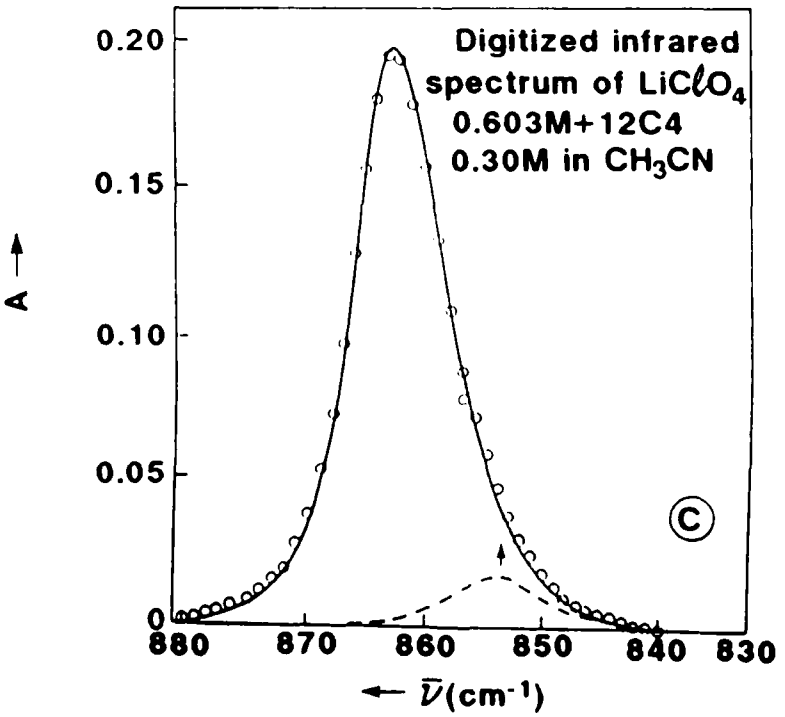
Digitized infrared
spectrum of LiClO4
0.603M+12C4
0.30M in CH3CN
A
C
ν̄(cm⁻¹)

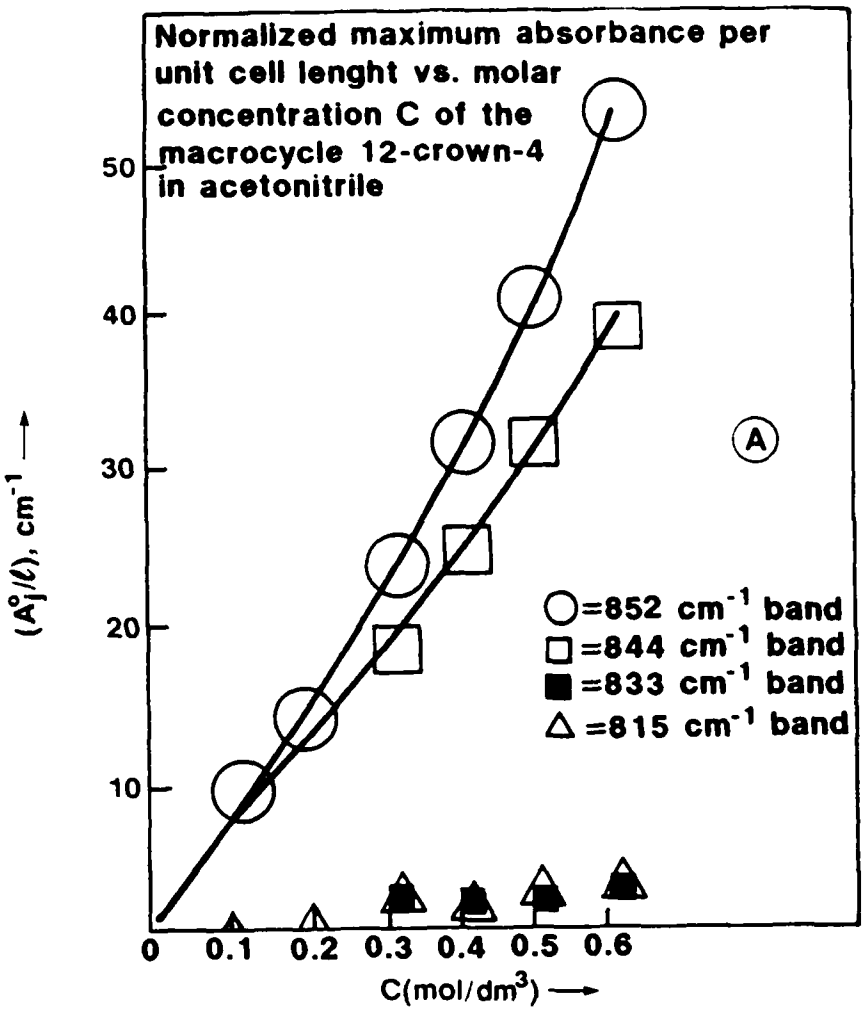
Normalized maximum absorbance per unit cell lenght vs. molar concentration C of the macrocycle 12-crown-4 in acetonitrile
(A°j/ℓ), cm-1
50
40
30
20
10
0
0.1
0.2
0.3
0.4
0.5
0.6
C(mol/dm3)
A
○=852 cm-1 band
□=844 cm-1 band
■=833 cm-1 band
△=815 cm-1 band

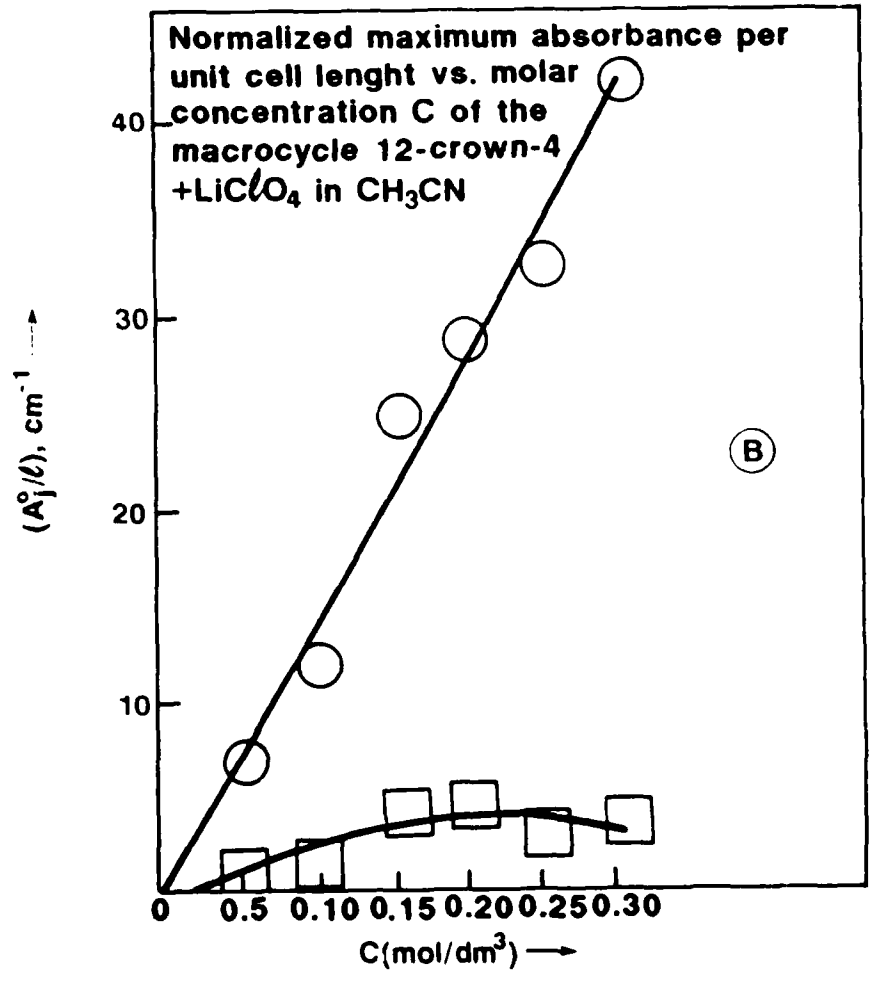
Normalized maximum absorbance per unit cell lenght vs. molar concentration C of the macrocycle 12-crown-4 +LiClO4 in CH3CN
(A°j/ℓ), cm-1
40
30
20
10
0
0.5
0.10
0.15
0.20
0.25
0.30
C(mol/dm3)
B

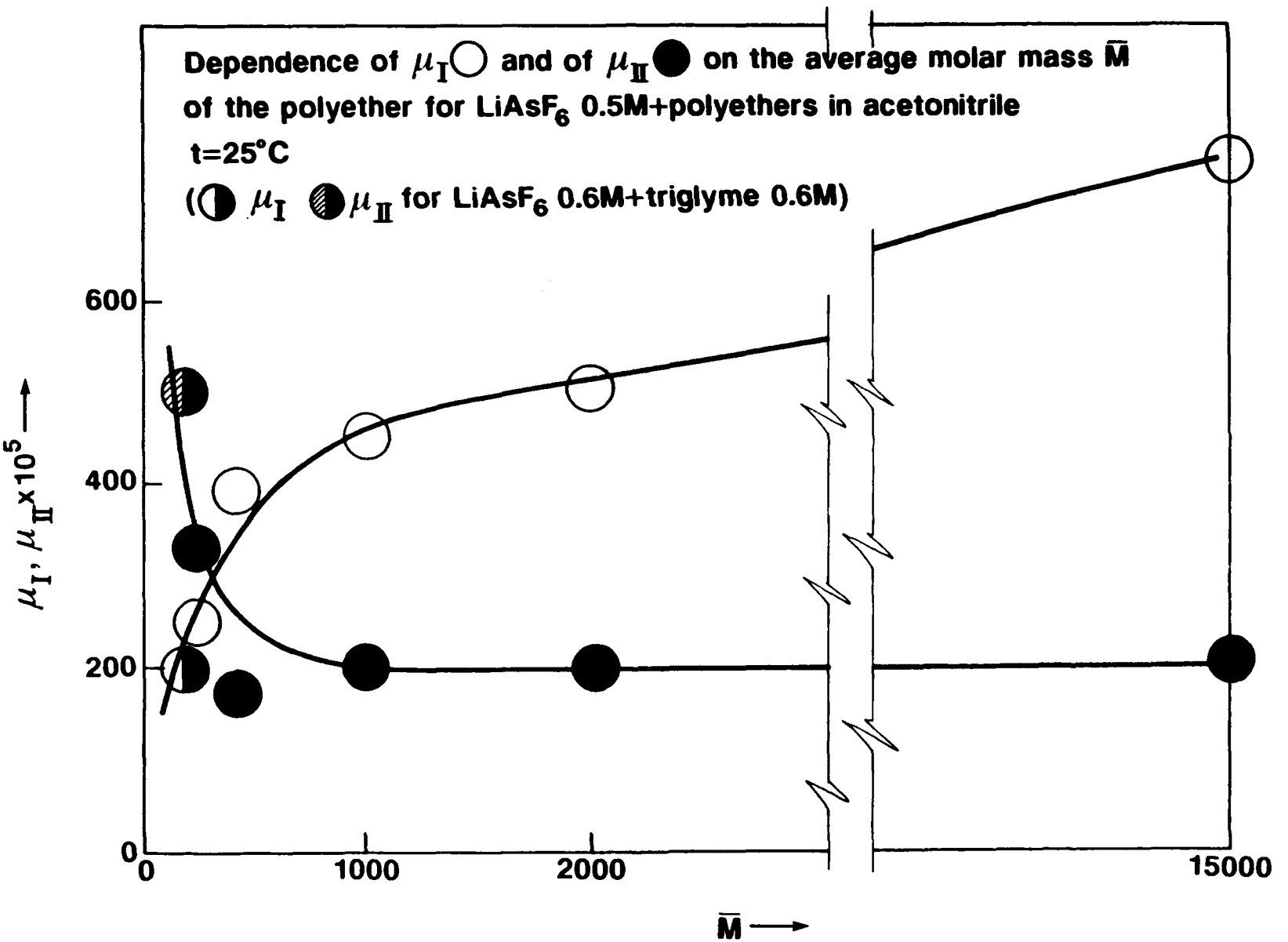
Dependence of μ_I ○ and of μ_{II} ● on the average molar mass $\bar{M}$
of the polyether for $LiAsF_6$ 0.5M+polyethers in acetonitrile
t=25°C
(◑ μ_I ◍ μ_{II} for $LiAsF_6$ 0.6M+triglyme 0.6M)
600
400
200
0
$\mu_I, \mu_{II} \times 10^5$ ⟶
0
1000
2000
15000
$\bar{M}$ ⟶

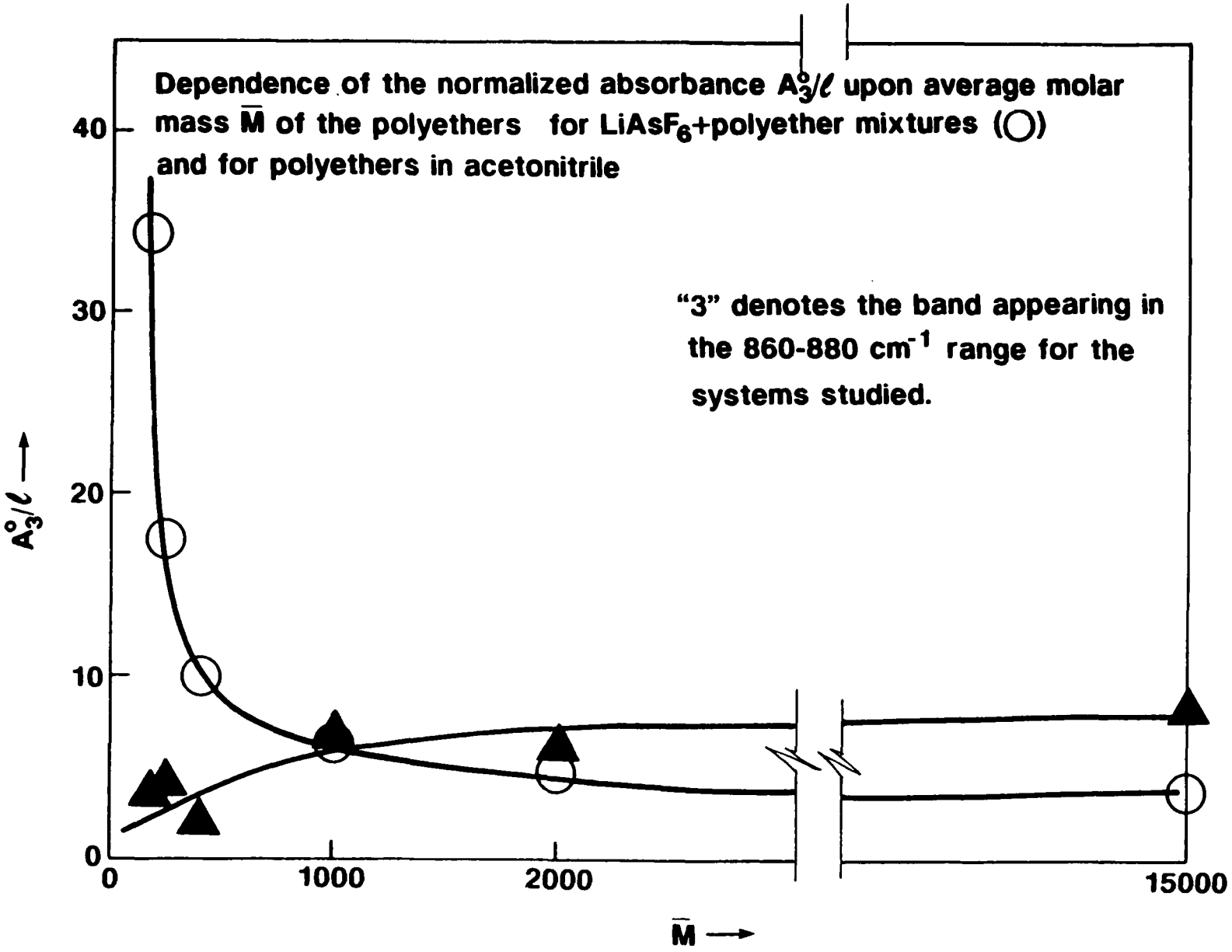
Dependence of the normalized absorbance A_3°/ℓ upon average molar mass $\bar{M}$ of the polyethers for $LiAsF_6$+polyether mixtures (○) and for polyethers in acetonitrile
"3" denotes the band appearing in the 860-880 cm^{-1} range for the systems studied.
40
30
20
10
0
A_3°/ℓ ⟶
0
1000
2000
15000
$\bar{M}$ ⟶

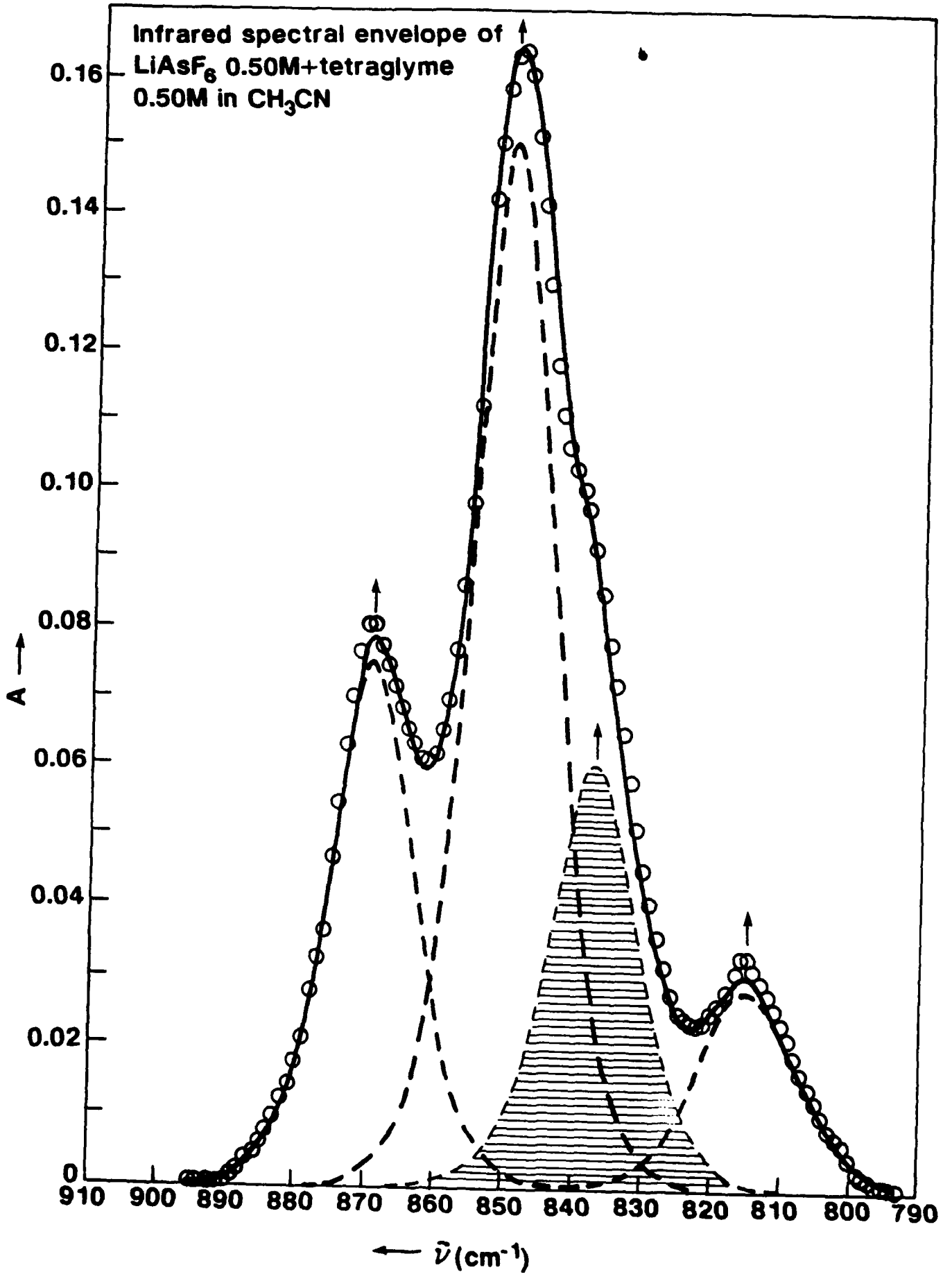
Infrared spectral envelope of
LiAsF6 0.50M+tetraglyme
0.50M in CH3CN
0.16
0.14
0.12
0.10
0.08
0.06
0.04
0.02
0
A
910 900 890 880 870 860 850 840 830 820 810 800 790
ν̃ (cm-1)

Microfilm Edition

Table I. Ultrasonic parameters μ_I, f_I, μ_{II}, f_{II}, B and sound velocity u for all the concentrations investigated of the systems $LiCl O_4$ or $LiAsF_6$ + Triglyme and $LiCl O_4$ or $LiAsF_6$ + polyethylene oxide (at R_{PEO} = 4.0 with R_{PEO} = $[-CH_2-CH_2-O-]/[Li^+]$) in the solvent CH_3CN at 25°C.

C_{LIX} (M)	C_{TG} (M)	Anion -	$\mu_I x10^5$ -	f_I (MHz)	$\mu_{II} x10^5$ -	f_{II} (MHz)	$Bx10^{17}$ ($cm^{-1}s^2$)	$ux10^{-5}$ ($cm\ s^{-1}$)
1.00	1.00	AsF_6^-	220	100	550	16	62	1.251
0.80	0.80	"	220	100	520	17	59	1.250
0.60	0.60	"	200	100	500	15	55	1.261
0.50	0.50	$Cl O_4^-$	250	100	500	12	56	1.308
0.40	0.40	$Cl O_4^-$	200	100	420	12	57	1.311
0.32	0.32	$Cl O_4^-$	110	90	400	12	60	1.300

C_{LIX} (M)	R_{PEO} -	Anion -	$\mu_I x10^5$ -	f_I (MHz)	$\mu_{II}NO^5$ -	f_{II} (MHz)	$Bx10^{17}$ ($cm^{-1}s^2$)	$ux10^{-5}$ ($cm\ s^{-1}$)
0.61	4.0	AsF_6^-	750	100	200	15	63	1.268
0.50	4.0	AsF_6^-	750	100	200	14	60	1.270
0.40	4.0	AsF_6^-	550	100	200	13	58	1.277
0.40	4.0	AsF_6^-	600	100	220	13	58	1.269
0.31	4.0	AsF_6^-	450	100	200	12	61	1.273
0.10	4.0	AsF_6^-	180	70	130	7	62	1.280

Microfilm Edition

0.32	4.0	ClO_4^-	500	100	350	12	53	1.288
0.20	4.0	ClO_4^-	300	100	280	9	58	1.284
0.15	4.0	ClO_4^-	210	90	200	7.5	61	1.287
0.076	4.0	ClO_4^-	170	55	100	4	62	1.283
0.050	4.0	ClO_4^-	100	45	70	2.8	63	1.283

C_{LIX}	C_{12C4}	Anion						
0.32	0.32	ClO_4^-	210	120	90	2	57	1.289

Microfilm Edition

Table II

Infrared parameters $\bar{\nu}_j^o$, $\bar{A}_j^o$ $(\Delta\bar{\nu}_{1/2})_J$ (J = 1,2,3) for the three Gaussian-Lorentzian bands used to deconvolute the spectral envelope of TG, $LiC\ell O_4$ + TG (R=1) $LiAsF_6$+TG (R=1), of PEO, $LiC\ell O_4$ + PEO (R_{PEO} = 4.0) and $LiAsF_6$ + PEO (R_{PEO} = 4.0) and of the macrocycle 12C4, $LiC\ell O_4$ + 12C4 in the solvent acetonitrile. Also reported are the IR cell lengths ℓ and, for each system, the normalized absorbances A_j^o/ℓ (to unit cell length) vs concentration functions[a]

C (M)	$\bar{\nu}_1^o$ (cm^{-1})	A_1^o -	$(\Delta\bar{\nu}_{1/2})_1$ (cm^{-1})	$\bar{\nu}_2^o$ (cm^{-1})	A_2^o -	$(\Delta\bar{\nu}_{1/2})_2$ (cm^{-1})	$\bar{\nu}_3^o$ (cm^{-1})	A_3^o -	$(\Delta\bar{\nu}_{1/2})_3$ $(cm^{-1})^3$	ℓ_{cell} cmx10^2
System: Triglyme in CH_3CN										
1.00	818.5	0.025	30	852.5	0.328	23.5	878.5	0.045	18.5	0.469
0.908	818	0.030	30	853	0.285	25	880	0.040	18	0.501
0.802	818	0.019	30	852.8	0.250	24	879	0.034	19.1	0.547
0.694	819	0.023	30	853	0.225	24	880	0.030	18	0.458
0.604	818	0.013	30	853	0.195	25	879	0.023	18	0.463
0.503	818	0.010	30	853	0.155	25	879	0.017	16	0.446
0.414	818	0.009	30	853	0.135	25	879	0.016	16	0.467
0.297	817	0.007	30	853	0.098	25	880	0.014	18	0.462

$\frac{1}{\ell} A^o_{853} = 0.246 + 64.7_1\ C \quad r^2 = 0.989$ [a]

$\frac{1}{\ell} A^o_{818} = -0.056 + 5.59\ C \quad r^2 = 0.943$ [a]

$\frac{1}{\ell} A^o_{879} = -0.032 + 8.83\ C \quad r^2 = 0.987$ [a]

a) Least squares performed giving 50% statistical weight to the intercepts.

Microfilm Edition

Table II (continued)

C_{LIX} (M)	C_{TG} (M)	$\bar{\nu}_1^o$ (cm^{-1})	A_1^o -	$(\Delta\bar{\nu}_{1/2})_1$ (cm^{-1})	$\bar{\nu}_2^o$ (cm^{-1})	A_2^o -	$(\Delta\nu_{1/2})_2$ (cm^{-1})	$\bar{\nu}_3^o$ (cm^{-1})	A_3^o -	$(\Delta\bar{\nu}_{1/2})_3$ (cm^{-1})	ℓ cell cm x 10^2
System: $LiClO_4$ + Triglyme in acetonitrile R = 1.0[b]											
0.900	0.901	813	0.022	16	843.5	0.310	14	870	0.240	14	0.447
0.804	0.804	813	0.019	16	843.5	0.265	15.5	870	0.210	14	0.448
0.698	0.693	812	0.016	16	843.5	0.235	15.5	870	0.185	13.5	0.445
0.603	0.603	813	0.011	15	843	0.220	15	870	0.170	14	0.510
0.506	0.503	813	0.012	16	843.5	0.175	15	870	0.140	14	0.463
0.407	0.412	813	0.009	16	844	0.150	15	870	0.110	14	0.501
0.299	0.299	813	0.006	16	844	0.095	15.5	870.5	0.074	16	0.467
System: $LiAsF_6$ + Triglyme in acetonitrile R = 1.0											
0.810	0.812	815.5	0.040	$16._8$	843.6	0.300	13.6	870	0.220	12.9	0.470
0.613	0.610	815.5	0.032	$16._8$	843.5	0.230	15.5	870	0.165	13.5	0.478
0.406	0.407	816	0.008	20	843.8	0.063	12.5	870	0.048	12.3	0.201

$\frac{1}{\ell} A^o_{813} = -0.061 + 5.1_0\, C, \qquad r^2 = 0.974$ [b]

$\frac{1}{\ell} A^o_{844} = -0.200 + 75.65\, C, \qquad r^2 = 0.999$ [b]

$\frac{1}{\ell} A^o_{870} = -0.252. + 58.41\, C, \qquad r^2 = 0.998$ [b]

b) Least squares performed on $LiClO_4$ + Triglyme data of A^o_J/ℓ, giving 50% statistical weight to the intercepts.

Microfilm Edition

Table II (continued)

System: PEO in CH_3CN

C_{PEO} [c] (M)	$\ell_{cell} \times 10^2$ (cm)	$\bar{\nu}_1^o$ (cm^{-1})	A_1^o -	$(\Delta\bar{\nu}_{1/2})_1$ (cm^{-1})	$\bar{\nu}_2^o$ (cm^{-1})	A_2^o -	$(\Delta\bar{\nu}_{1/2})_2$ (cm^{-1})	$\bar{\nu}_3^o$ (cm^{-1})	A_3^o -	$(\Delta\bar{\nu}_{1/2})_3$ (cm^{-1})
0.900	0.417	810	0.016	27	845	0.128	29	865	0.048	22
0.804	0.440	811	0.015	26	844.5	0.120	27	865	0.050	22
0.700	0.446	811	0.009	26	844.5	0.089	26	862	0.037	21
0.600	0.446	811	0.010	26	845	0.084	27	864	0.038	22
0.501	0.422	811	0.004	26	844.5	0.073	27	864.5	0.035	22
0.400	0.436	812	0.006	26	844	0.053	25	864	0.030	25
0.301	0.461	811	0.007	26	844	0.043	25	865	0.024	25

$$\frac{1}{\ell} A^o_{811} = -0.036 + 3.7_6\ C \quad r^2 = 0.927\ ^a$$

$$\frac{1}{\ell} A^o_{844} = -0.13 + 32.6_6\ C \quad r^2 = 0.992\ ^a$$

$$\frac{1}{\ell} A^o_{864} = 0.23 + 13.5_0\ C \quad r^2 = 0.975\ ^a$$

c) The concentration C_{PEO} is expressed as the molarity of the moiety $(-O-CH_2-CH_2-)_4$ of formal molar mass = 4x44.054 = 176.22 grams.

Microfilm Edition

Table II (continued)

System: $LiCl O_4$ + PEO in CH_3CN

C_{LIX} (M)	R_{PEO} -	$\bar{\nu}_1^o$ (cm^{-1})	A_1^o -	$(\Delta\bar{\nu}_{1/2})_1$ (cm^{-1})	$\bar{\nu}_2^o$ (cm^{-1})	A_2^o -	$(\Delta\bar{\nu}_{1/2})_2$ (cm^{-1})	$\bar{\nu}_3^o$ cm^{-1}	A_3^o -	$(\Delta\bar{\nu}_{1/2})_3$ (cm^{-1})	ℓ_{cell} $x10^2$, cm
0.710	4.0	812	0.017	18	843	0.087	28	862	0.030	18	0.445
0.607	4.0	814	0.013	17	843	0.075	26	863	0.028	17	0.439
0.509	4.0	812.5	0.011	18	844	0.063	28	863.5	0.020	18	0.436
0.404	4.0	811.5	0.008	18	844.3	0.050	28	863.5	0.012	18	0.447
0.301	4.0	812	0.03_5	15	843.5	0.030	22	862	0.012	23	0.434
System: $LiAsF_6$ + PEO in CH_3CN											
0.909	4.0	814.5	0.059	16	844	0.122	28	864	0.033	16	0.486
0.709	4.0	814.5	0.045	17	844	0.092	27	864	0.025	18	0.490
0.601	4.0	814.5	0.034	15	844	0.077	28	864	0.018	15	0.483
0.500	4.0	815	0.029	15	$844._5$	0.063	26	864	0.017	16	0.460
0.301	4.0	815	0.005_5	14	845	0.017	25	865	0.0038	15	0.250

$\frac{1}{\ell} A^o_{812-815} = -0.346 + 10.03\ C \qquad r^2 = 0.78_5$ [d]

$\frac{1}{\ell} A^o_{844} = -0.120 + 27.3_7\ C \qquad r^2 = 0.997$ [d]

$\frac{1}{\ell} A^o_{864} = -0.025 + 8.02\ C \qquad r^2 = 0.947$ [d]

d) least squares applied to both $LiCl O_4$ + PEO and $LiAsF_6$ + PEO data giving 50% statistical weight to the intercept.

Microfilm Edition

Table II (continued)

System: 12C4 in CH_3CN

C_{12C4} (M)	$\bar{\nu}_1^o$ (cm^{-1})	A_1^o -	$(\Delta\bar{\nu}_{1/2})_1$ (cm^{-1})	$\bar{\nu}_2^o$ (cm^{-1})	A_2^o [e] -	$(\Delta\bar{\nu}_{1/2})_2$ (cm^{-1})	$\bar{\nu}_3^o$ (cm^{-1})	A_3^o -	$(\Delta\bar{\nu}_{1/2})_3$ (cm^{-1})	$\bar{\nu}_4^o$ (cm^{-1})	A_4^o -	$(\Delta\bar{\nu}_{1/2})_4$ (cm^{-1})	$\ell_{cell} \times 10^2$ (cm)
0.601	815	0.014	6	832.3	0.012	7	843.6	0.176	6.25	850.8	0.246	9.7	0.456
0.493	815	0.013	6	833.3	0.009	6	843.8	0.144	7.8	851.4	0.185	9.1	0.450
0.401	815	0.010	6	833.3	0.008	6	844	0.125	7.9	851.5	0.146	9.6	0.504
0.313	815	0.008	6	836	0.009	6.5	844	0.083	6.9	851.3	0.109	9.2	0.451
0.201	815	0.003	6	-	-	-	844	0.069	7.9	851.6	0.070	8.6	0.505
0.111	815	0.002	6	-	-	-	844	0.040	6.8	851.5	0.045	7.2	0.487

$$\frac{1}{\ell} A^o_{815} = -0.0048 - 1.884\ C + 32.32\ C^2 - 34.24\ C^3, \qquad r^2 = 0.992\ ^e$$

$$\frac{1}{\ell} A^o_{844} = 0.0404 + 76.75\ C - 74.11\ C^2 + 92.37\ C^3, \qquad r^2 = 0.998\ ^e$$

$$\frac{1}{\ell} A^o_{851} = 0.0323 + 82.82\ C - 74.78\ C^2 + 144.5\ C^3, \qquad r^2 = 0.998\ ^e$$

e) The band centered at $\bar{\nu}^o \simeq 833\ cm^{-1}$ is visible only for C > 0.20 M. Hence the (A_3^o/ℓ) data have not been fitted by interpolation functions.

Microfilm Edition

Table II (continued)

System: $LiClO_4$+12C4 in CH_3CN

C_{12C4}	C_{LiClO_4}	$\bar{\nu}_1^o$	A_1^o	$(\Delta\bar{\nu}_{1/2})_1$	$\bar{\nu}_2^o$	A_2^o	$(\Delta\bar{\nu}_{1/2})_2$	ℓ cell$\times 10^2$
(M)	(M)	(cm^{-1})	(cm^{-1})	-	(cm^{-1})	-	(cm^{-1})	(cm)
System: $LiClO_4$ + 12C4 in CH_3CN								
0.304	0.601	853.8	0.016	9	862.4	0.196	9	0.461
0.252	0.505	854.1	0.013	8.2	862.4	0.155	9.4	0.472
0.200	0.404	855.8	0.0225	9	863	0.147	7	0.511
0.161	0.325	855.5	0.020	9	863	0.123	6.9	0.490
0.0978	0.201	855.5	0.007	8	862.5	0.056	9.2	0.468
0.051	0.102	855.3	0.004	6	862.8	0.032	7	0.467

$$\frac{1}{\ell} A^o_{855} = -0.0274 + 16.904\ C + 78.429\ C^2 - 331.0\ C^3, \qquad r^2 = 0.921\ ^a$$

$$\frac{1}{\ell} A^o_{863} = -0.0065 + 138.98\ C, \qquad r^2 = 0.9941\ ^a$$

Microfilm Edition

Table III. Ultrasonic parameters μ_I, f_I, μ_{II}, f_{II}, B and sound velocity u for the concentrations 0.5 M of $LiAsF_6$ + Tetraglyme molar ratio (Tetraglyme/$LiClO_4$) = 1 and of 0.5 M $LiAsF_6^-$ + PEO, 400, 1000, 2000 at R = [-(CH_2-CH_2-O-)]/[Li^+] = 4 in the solvent CH_3CN at 25°C.

C $LiAsF_6$ (M)	R	$\mu_I \times 10^5$	f_I(MHz)	$\mu_{II} \times 10^5$	f_{II}(MHz)	$B \times 10^{17}$ (cm^{-1} s^2)	$u \times 10^{-5}$ cm s^{-1}	Ligand
0.50	C = 0.50	250	100	330	12	52	1.272	Tetragl.
0.50	4.0	400	100	170	16	52	1.268	PEO (400)
0.50	4.0	450	80	200	15	62	1.281	PEO (1000)
0.50	4.0	500	90	200	15	63	1.265	PEO (2000)

Microfilm Edition

Table IV. Infrared parameters $\bar{\nu}_j^o$, A_j^o, $(\Delta\bar{\nu}_{1/2})_j$ (j=1,2,3,4) for $LiAsF_6$ 0.50 M + tetraglyme 0.50 M and (j = 1, 2, 3) for $LiAsF_6$ 0.50 M + PEO (400), PEO (1,000), PEO (2000) at R = $[-O-CH_2-CH_2-]/[Li]$ = 4 in acetonitrile. Same parameters for Tetraglyme and the PEO of molar masses 400, 1000, 2000 in CH_3CN. The spectral envelopes have been deconvoluted into four Gaussian-Lorentzian product functions for $LiAsF_6$ + Tetraglyme and into three Gaussian-Lorentzian products functions for $LiAsF_6$ + PEO of the above average molar masses.

System: Tetraglyme 0.50 + $LiAsF_6$ 0.50 in CH_3CN

$\bar{\nu}_1^o$ (cm^{-1})	A_1^o -	$(\Delta\bar{\nu}_1)_{1/2}$ (cm^{-1})	$\bar{\nu}_4^o$ (cm^{-1})	A_4^o	$(\Delta\bar{\nu}_4)_{1/2}$ (cm^{-1})	$\bar{\nu}_2^o$ (cm^{-1})	A_2^o -	$(\Delta\bar{\nu}_2)_{1/2}$ (cm^{-1})	$\bar{\nu}_3^o$ (cm^{-1})
815	0.029	16	837	0.06	15	849	0.15	14	869

A_3^o -	$(\Delta\bar{\nu}_3)_{1/2}$ (cm^{-1})	$\ell_{cell} \times 10^2$ (cm)
0.075	14	0.425

Microfilm Edition

Table IV (cont.)

$\bar{\nu}_1^o$ (cm^{-1})	A_1^o -	$(\Delta\bar{\nu})_{1\,1/2}$ (cm^{-1})	$\bar{\nu}_2^o$ (cm^{-1})	A_2^o -	$(\Delta\bar{\nu})_{2\,1/2}$ (cm^{-1})	$\bar{\nu}_3^o$ (cm^{-1})	A_3^o -	$(\Delta\bar{\nu})_{3\,1/2}$ (cm^{-1})	ℓ cell (cm)
System: PEO (400) + $LiAsF_6$ 0.50 M, R = 4.0									
813	0.019	16	843	0.077	25	862.5	0.045	22	0.449
System: PEO (1000) + $LiAsF_6$ 0.50 M; R = 4.0									
814	0.022	20	842.5	0.068	26	862.5	0.030	22	0.457
System: PEO (2000) + $LiAsF_6$ 0.50 M; R = 4.0									
814	0.023	20	843	0.06	27	862.5	0.022	21	0.457

Microfilm Edition

Table IV (cont.)

$\bar{\nu}_1^o$ (cm^{-1})	A_1^o -	$(\Delta\bar{\nu}_{1/2})_1$ (cm^{-1})	$\bar{\nu}_2^o$ (cm^{-1})	A_2^o -	$(\Delta\bar{\nu}_{1/2})_2$ (cm^{-1})	$\bar{\nu}_3^o$ (cm^{-1})	A_3^o -	$(\Delta\bar{\nu}_{1/2})_3$ (cm^{-1})	$\ell_{cell} \times 10^2$ (cm)
System: Tetraglyme 0.50 M in CH_3CN									
819	0.011	30	851	0.155	27	874	0.018	16	0.432
System: PEO (400) 0.502 M [a] in CH_3CN									
819	0.008	30	851	0.11	27	871	0.008	20	0.463
System: PEO (1000) 0.50_5 M[a] in CH_3CN									
815.5	0.009	20	846.5	0.074	27	864	0.028	22	0.422
System: PEO (2000) 0.50_3 M[a] in CH_3CN									
813	0.007	20	845	0.071	27	864	0.029	22	0.452

a) The term molarity (M) here is intended as the weight of polymer in gram divided by the mass of the molecular unit $(-O-CH_2-CH_2-)_4$ per dm^3 of solution.